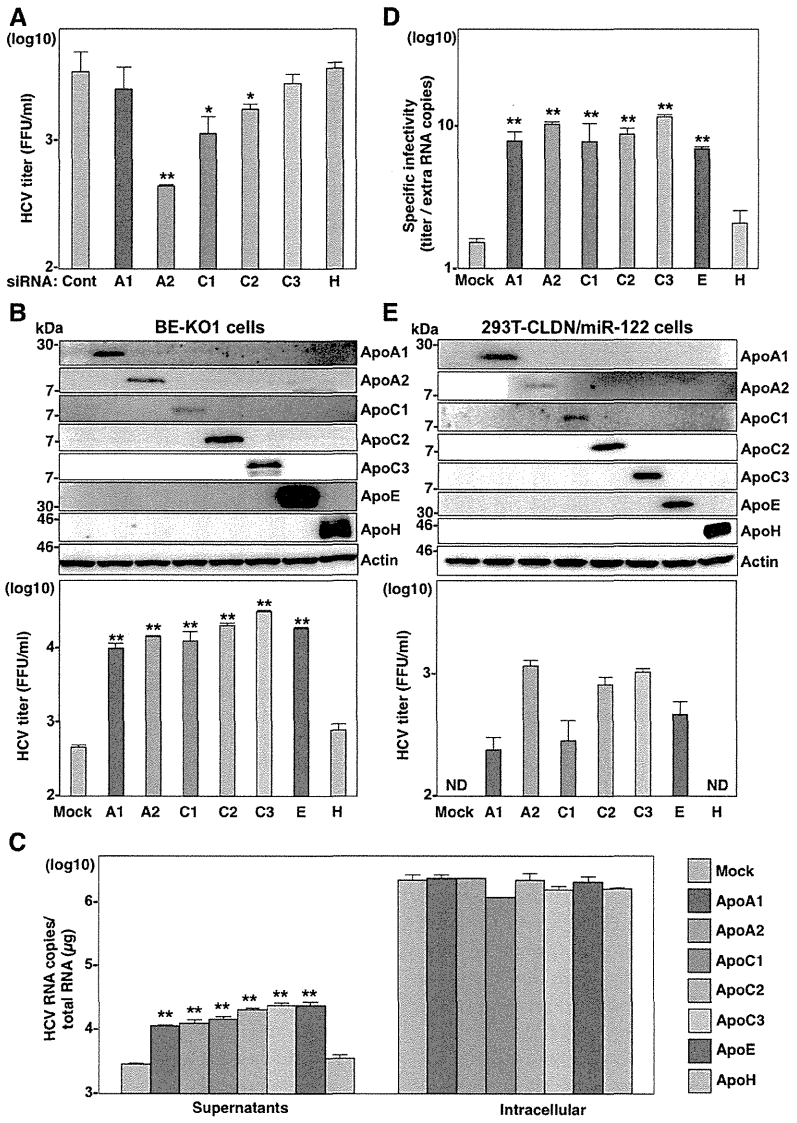

Figure 4. Exchangeable apolipoproteins redundantly participate in the formation of infectious HCV particles. (A) BE-KO1 cells infected with HCVcc at an MOI of 1 at 6 h post-transfection with siRNAs targeting ApoA1 (A1), ApoA2 (A2), ApoC1 (C1), ApoC2 (C2), ApoC3 (C3) and ApoH (H) and infectious titers in the culture supernatants were determined by focus-forming assay at 72 h post-infection. (B) ApoA1, ApoA2, ApoC1, ApoC2, ApoC3, ApoE and ApoH were exogenously expressed in BE-KO1 cells by infection with lentiviral vectors, and then infected with HCVcc at an MOI of 1. Expression of the apolipoproteins was determined by immunoblot analysis (upper), and infectious titers in the culture supernatants were determined at 72 h post-infection by focus-forming assay (lower). (C) Extracellular and intracellular HCV RNA in BE-KO1 cells expressing apolipoproteins and infected with HCVcc were determined at 72 h post-infection by qRT-PCR. (D) Specific infectivity was calculated as extracellular infectious titers/ extracellular HCV RNA copies in BE-KO1 cells expressing apolipoproteins at 72 h post-infection. (E) 293T cells stably expressing CLDN1 and miR-122 (293T-CLDN/miR-122 cells) were infected with the lentiviral vectors, and the expressions of the apolipoproteins were determined by immunoblot analysis (upper). These cells were infected with HCVcc at an MOI of 1, and infectious titers in the supernatants were determined at 72 h post-infection by focus-forming assay (lower). In all cases, asterisks indicate significant differences (*, $P<0.05$; **, $P<0.01$) versus the results for control cells.
doi:10.1371/journal.ppat.1004534.g004

ER membrane, in contrast to the co-localization of core proteins of HCVcc (JFH1) with LD (Fig. 6E upper). However, core proteins were accumulated around LD in BE-KO1 cells infected with HCVcc/Jc1, as seen in those infected with HCVcc (JFH1) (Fig. 6E lower). These results suggest that apolipoproteins participate in the steps of HCV particle formation occurring after HCV protein assembly on the LD.

To further examine the involvement of apolipoproteins in the infectious particle formation of HCV, culture supernatants and cell lysates of BE-KO1 and ApoE-res cells infected with HCVcc were analyzed by buoyant density ultracentrifugation (Fig. 7A–B) [28]. Secretion of viral capsids in the supernatants was severely impaired in BE-KO1 cells in comparison with that in ApoE-res cells (Fig. 7A upper), in contrast to the detection of abundant intracellular capsids in both cell lines (Fig. 7B upper). Although peak levels of the core proteins and infectious titers were detected around 1.08 g/ml in both cell lines, the infectious titers in all fractions of BE-KO1 cells were significantly lower than those in ApoE-res cells, supporting the notion that apolipoproteins participate in the post-assembly process of HCV capsids which

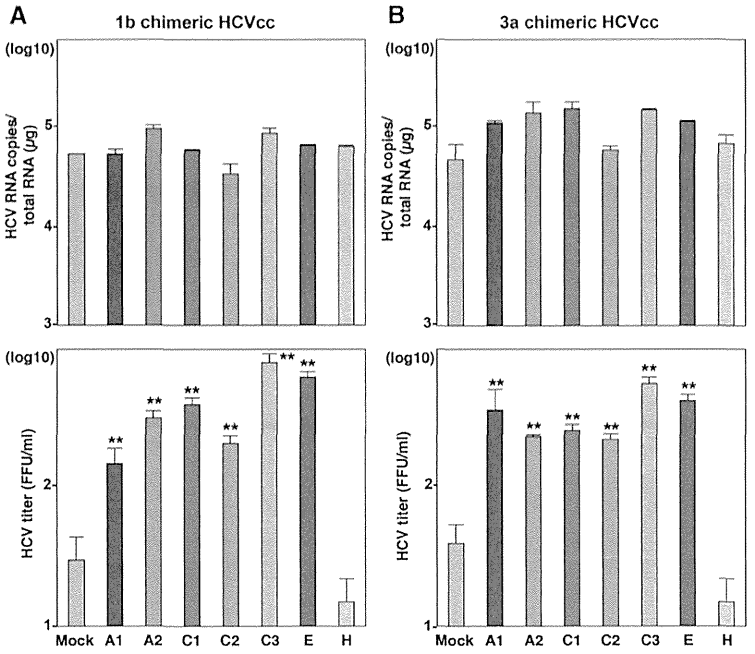

Figure 5. Exchangeable apolipoproteins participate in the formation of infectious HCV particles of genotype 1 and 3. ApoA1, ApoA2, ApoC1, ApoC2, ApoC3, ApoE and ApoH were exogenously expressed in BE-KO1 cells by infection with lentiviral vectors, and then infected with genotype 1b and 3a chimeric HCVcc, TH/JFH1 (A) and S310/JFH1 (B) at an MOI of 0.5. Intracellular HCV RNA and infectious titers in the culture supernatants were determined at 72 h post-infection by qRT-PCR (upper) and focus-forming assay (lower). Asterisks indicate significant differences (**, $P<0.01$) versus the results for control cells.
doi:10.1371/journal.ppat.1004534.g005

is required to confer infectivity. Next, to examine the involvement of apolipoproteins in the envelopment of HCV particles, lysates of BE-KO1 and ApoE-res cells infected with HCVcc were treated with proteinase K in the presence or absence of Triton X [26]. Protection of HCV core proteins from the protease digestion was observed in both cell lysates (Fig. 7C), suggesting that apolipoproteins are not involved in the envelopment of HCV particles. Collectively, these results suggest that exchangeable apolipoproteins participate in the post-envelopment step of HCV particle formation.

Amphipathic α-helices in exchangeable apolipoproteins participate in the formation of infectious HCV particles through the interaction with viral particles

To determine the structural relevance of apolipoproteins involved in the HCV assembly, the secondary structures of the apolipoproteins were deduced by using a CLC Genomics Workbench and previous reports (Fig. 8A) [29–34]. Tandem repeats of amphipathic α-helices were observed in the apolipoproteins capable of rescuing HCV assembly in BE-KO1 cells, but not in those lacking this activity, suggesting that amphipathic α-helices in the apolipoproteins participate in the assembly of HCV. To examine the involvement of the amphipathic α-helices of the exchangeable apolipoproteins in the particle formation of HCV, we constructed expression plasmids encoding deletion mutants of ApoE and ApoC1, and then these deletion mutants were exogenously expressed in BE-KO1 cells by lentiviral vectors (Fig. 8B and C upper panels). The expression of all of the deletion mutants of ApoE and ApoC1 containing either N-terminal or C-terminal amphipathic α-helices rescued the particle formation of HCV in BE-KO1 cells (Fig. 8B and C lower panels), suggesting that amphipathic α-helices in the apolipoproteins play crucial roles in the production of infectious HCV particles. In addition, more abundant full-length and truncated ApoE were detected in the precipitates of the culture supernatants of cells infected with HCVcc than those of mock-infected cells concentrated by ultracentrifugation, suggesting that the amphipathic α-helices of apolipoproteins are directly associated with HCV particles (Fig. 8D and E). Taken together, the data in this study strongly suggest that exchangeable apolipoproteins redundantly participate in the infectious particle formation of HCV through the interaction between amphipathic α-helices and viral particles.

Discussion

In this study, we demonstrated the redundant roles of ApoB and the exchangeable apolipoproteins ApoA1, ApoA2, ApoC1, ApoC2, ApoC3 and ApoE in the assembly of infectious HCV particles. The deficiencies of both ApoB and ApoE inhibited the production of infectious HCV particles in Huh7 cells, and exogenous expression of exchangeable apolipoproteins rescued the particle formation. cDNA microarray revealed that the expression patterns of exchangeable apolipoproteins in hepatic cancer cell lines are widely different from those in liver tissue. In previous reports, ApoE and ApoB were identified as important host factors for the assembly of infectious HCV particles [10,11], and knockdown of ApoE and ApoB expression also inhibited the production of infectious particles in this study. Because ApoB and ApoE are major apolipoproteins in VLDL, several reports have suggested that the VLDL production machinery participates in the production of HCV particles. Furthermore, density gradient analyses revealed co-fractionation of HCV RNA with lipoproteins, with the resulting complexes being termed lipoviroparticles (LVP) [12,35]. However, it has been reported that there is no correlation between secretion of VLDL and production of LVP [36]. In

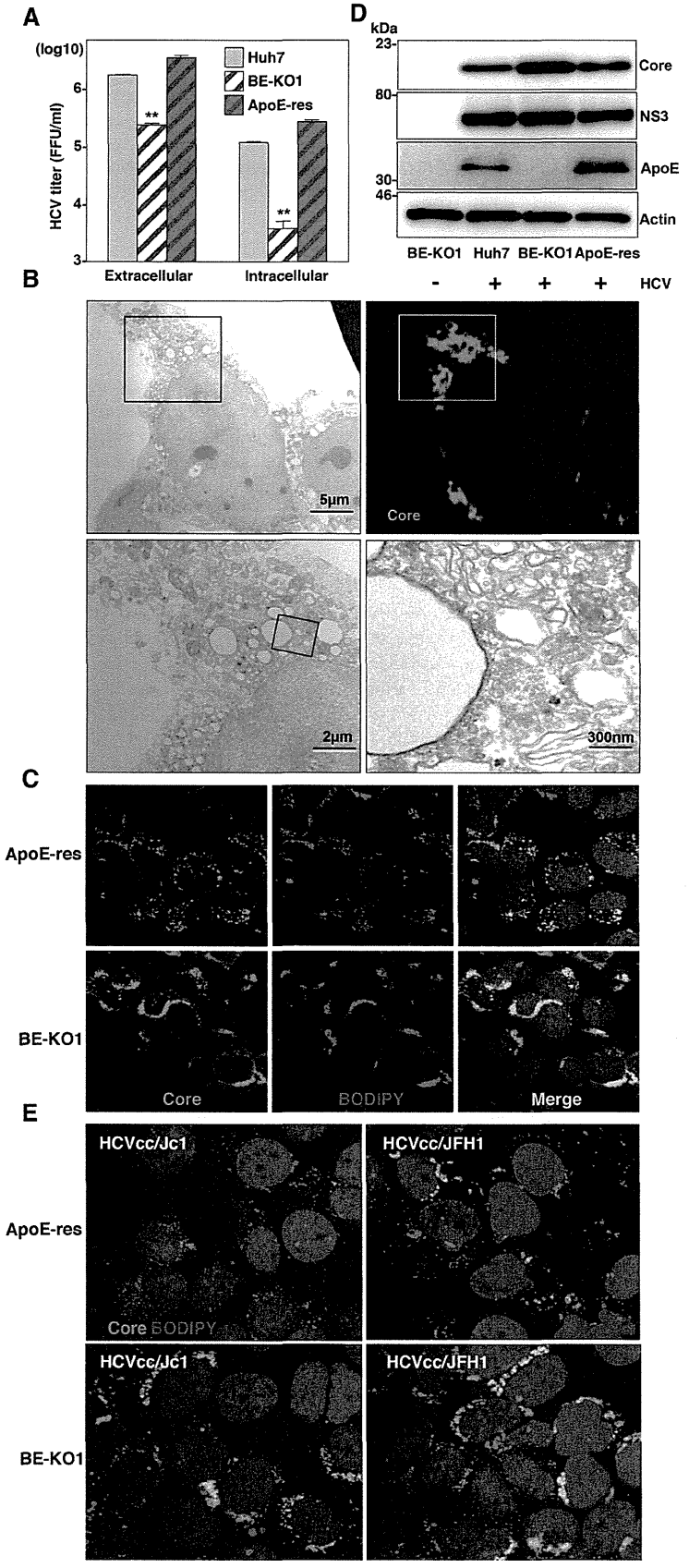
A
(log10)
HCV titer (FFU/ml)
6
5
4
3
Huh7
BE-KO1
ApoE-res
**
**
Extracellular
Intracellular
D
kDa
23
80
30
46
Core
NS3
ApoE
Actin
BE-KO1 Huh7 BE-KO1 ApoE-res
- + + + HCV
B
5μm
Core
2μm
300nm
C
ApoE-res
BE-KO1
Core
BODIPY
Merge
E
HCVcc/Jc1
HCVcc/JFH1
ApoE-res
Core BODIPY
HCVcc/Jc1
HCVcc/JFH1
BE-KO1

Figure 6. Accumulation of core proteins around lipid droplets in BE-KO1 cells. (A) Extracellular and intracellular infectious titers in Huh7, BE-KO1 and ApoE-restored cells infected by lentiviral vector (ApoE-res) were determined at 72 h post-infection with HCVcc at an MOI of 1 by focus-forming assay. Asterisks indicate significant differences (**, $P<0.01$) versus the results for parental cells. (B) BE-KO1 cells infected with HCVcc at an MOI of 1 were stained with anti-Core antibody at 72 h post-infection and examined by fluorescence microscopy. Identical fields were observed under electron microscopy by using the correlative FM-EM technique. The boxed areas are magnified and displayed. Huh7, BE-KO1 and ApoE-res cells infected with HCVcc at an MOI of 1 were subjected to immunofluorescence analyses by using anti-Core antibody (C), and immunoblotting by using antibodies against Core, NS3, ApoE, and actin at 72 h post-infection (D). Lipid droplets and cell nuclei were stained by BODIPY and DAPI, respectively. (E) BE-KO1 and ApoE-res cells infected with Jc1 strain-based HCVcc (HCVcc/Jc1; left panel) or JFH1 strain-based HCVcc (HCVcc/JFH1; right panel) at an MOI of 1 were subjected to immunofluorescence analysis by using anti-Core antibody at 72 h post-infection. Lipid droplets and cell nuclei were stained by BODIPY and DAPI, respectively.
doi:10.1371/journal.ppat.1004534.g006

addition, exogenous expression of ApoE facilitated the infectious particle formation of HCV in 293T cells stably expressing CLDN1 and miR-122 [16], suggesting that ApoE-mediated particle formation is independent from VLDL production. Furthermore, exogenous expression of ApoA1, a major apolipoprotein of HDL, also facilitated the production of HCV particles as shown in Fig. 4E. These data suggest that the roles of the exchangeable apolipoproteins in HCV assembly are independent from the production of VLDL. MTTP plays crucial roles in the lipoprotein formation through the incorporation of triglyceride into growing lipoprotein and secretion of ApoB [21]. Although it has been shown that treatment with an MTTP inhibitor impairs the production of HCV particles [11], in this study, we found that knockout of MTTP abrogated the secretion of ApoB but not the production of infectious HCV particles. Collectively, these data suggest that exchangeable apolipoproteins redundantly participate in the infectious particle formation of HCV independently from lipoprotein secretion machinery.

Production of HCV capsids in the culture supernatants is impaired in 293T cells expressing miR-122 due to lack of ApoE expression, but envelopment of viral capsids is observed [37], suggesting that ApoE is involved in the post-envelopment step. Coller et al. suggested that ApoE is associated with *de novo* formation of HCV particles during secretory pathway based on an experiment using HCV possessing a tetracysteine-tag in the core protein [38]. In this study, ApoA1, ApoA2, ApoC1, ApoC2, ApoC3 and ApoE enhanced the formation of HCV particles in the post-envelopment step. These results suggest that a direct interaction between exchangeable apolipoproteins and enveloped particles in the ER lumen facilitates an efficient secretion of infectious HCV particles. Ultrastructural analysis of HCV particles has shown that large amounts of apolipoproteins, including ApoA1, ApoB and ApoE, bind to the surface of viral particles [39]. Interestingly, ApoE-specific antibodies were more efficient in capturing viral particles than α-E1/E2 antibodies, and significantly large numbers of gold particles reacting with ApoE were observed per virion than those with E2, suggesting that viral envelope proteins are masked by a large amount of apolipoproteins. The unique characteristics of interaction between apolipoproteins and HCV particles might be applied for visualization of entry and purification of HCV particles by using GFP- or affinity-tagged amphipathic α-helices of apolipoproteins. In the previous report, virocidal amphipathic helical peptides impaired the infectivity of viral particles [40]. There is a possibility that such peptide influences on the interaction between apolipoproteins and viral particles, and might be a new therapeutic approach.

In previous reports, the importance of the interaction between lipoprotein receptors and ApoE in the entry of HCV has been well established. Lipoprotein receptors including scavenger receptor class B type 1 (SR-B1) and low-density lipoprotein receptor (LDLR) are involved in HCV entry into the target cells [41,42]. LDLR is thought to mediate cell attachment of HCV through an interaction with virus associated ApoE [43,44]. SR-B1 also interacts with ApoE and hypervariable region 1 (HVR1) in the envelope protein of HCV [43]. In this study we have shown that exchangeable apolipoproteins including not only ApoE but also ApoA and ApoC facilitate the production of infectious HCV particles, and that exchangeable apolipoproteins directly associate with viral particles. Meunier et al. reported that ApoC1 associates intracellularly with viral particles during particle morphogenesis and enhances the entry of HCV through an interaction of the C-terminal region of ApoC1 with heparan sulfate [45]. Another group also showed that ApoC1 enhances HCV infection through the triple interplay among HVR1, ApoC1, and SR-B1 [46]. These results suggest that the interaction of HCV particles with apolipoproteins also participates in the entry through the binding of lipoprotein receptors including SR-B1 and LDLR.

Although the gene-knockout technique is essential to obtain reproducible and reliable data, and many knockout mice have been produced in various research areas, the development of experimental tools for HCV study has also been hampered by the narrow cell tropism [47,48]. A humanized mouse model in which human liver cells were xenotransplanted into immunodeficient mouse was developed and provided an important platform for the analysis of pathogenesis and the development of antivirals for HCV [49]. However, the exogenous expression of human receptor molecules required for HCV entry and impairment of innate immunity are required for the complete propagation of HCV in mice [50]. Gene-knockout techniques using a CRISPR/Cas9 system composed of guide RNA and Cas9 nuclease that form RNA-protein complexes to cleave the target sequences [19] have allowed quick and easy establishment of gene-knockout mice and cancer cell lines [51,52], and indeed, such MTTP-knockout cell lines were established also in this study. Recently, the high-throughput screening of host factors involved in several conditions was reported by using a CRISPR/Cas9 system [53]. Together, these novel genome-editing techniques are expected to reveal the precise roles of host factors involved in the HCV life cycle.

In summary, we have shown that apolipoproteins, including ApoA1, ApoA2, ApoC1, ApoC2, ApoC3, ApoE and ApoB, possess redundant roles in the assembly of HCV through the interaction of the amphipathic α-helices in the apolipoproteins with viral particles in the post-envelopment step. It is hoped that these findings will provide clues to the life cycle of HCV and assist in the development of novel antivirals targeting the assembly process of HCV.

Materials and Methods

NextBio Body Atlas

The NextBio Body Atlas application presents an aggregated analysis of gene expression across various normal tissues, normal cell types, and cancer cell lines [20]. It enables us to investigate the expression of individual genes as well as gene sets. Samples for Body Atlas data are obtained from publicly available studies that are internally curated, annotated, and processed. Body Atlas

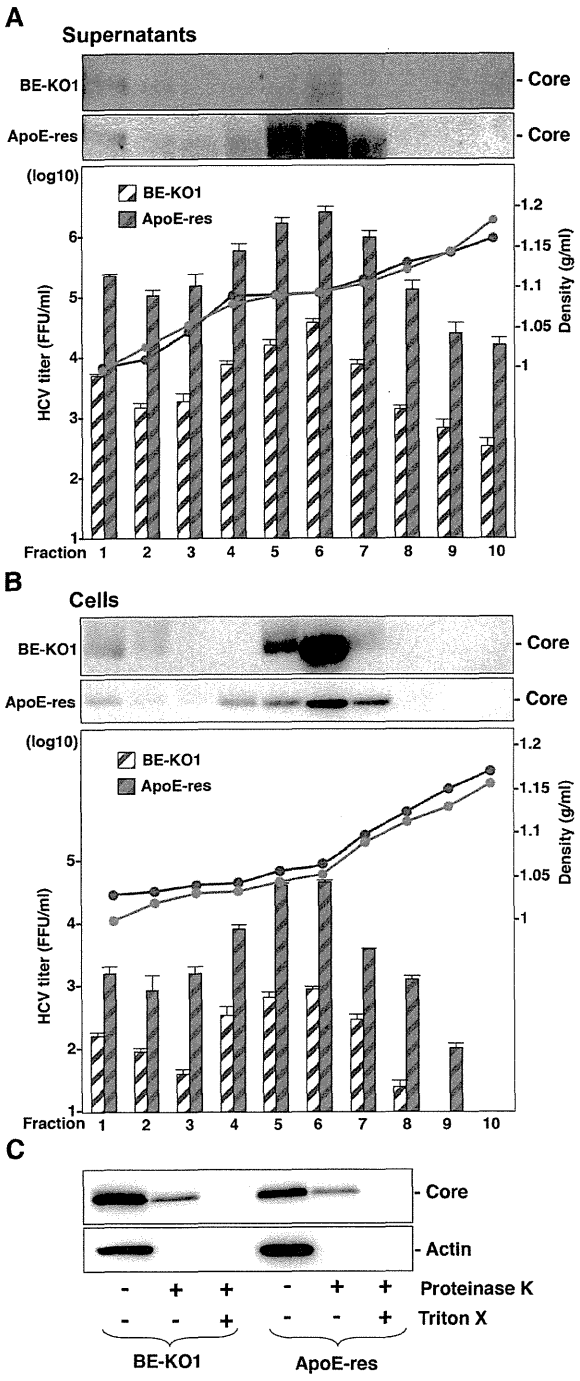

Figure 7. Apolipoproteins participate in the post-envelopment step of the HCV life cycle. The supernatants (A) and lysates (B) of BE-KO1 and ApoE-restored (ApoE-res) cells infected with HCVcc at an MOI of 1 were subjected to density gradient fractionation. Each fraction was subjected to immunoblotting using anti-Core antibody (upper). The infectious titers and densities of each fraction were determined (lower). (C) The lysates of BE-KO1 and ApoE-res cells infected with HCVcc at an MOI of 1 were subjected to proteinase K digestion protection assay. Lysates were separated into 3 parts and incubated for 1 h on ice in the presence or absence of 50 μg/ml proteinase K with/without pretreatment with 5% Triton-X and then subjected to immunoblotting.
doi:10.1371/journal.ppat.1004534.g007

measurements are generated from all available RNA expression studies that used Affymetrix U133 Plus or U133A Genechip Arrays for human studies. The results from 128 human tissue samples were incorporated from 1,067 arrays; 157 human cell types from 1,474 arrays; and 359 human cancer cell lines from 376 arrays. Gene queries return a list of relevant tissues or cell types rank-ordered by absolute gene expression and grouped by body systems or across all body systems. In the current analysis, we determined the expression levels of the apolipoproteins ApoA1, ApoA2, ApoB, ApoC1, ApoC2, ApoC3, ApoD, ApoE, ApoH, ApoL1, ApoL2 and ApoO in liver tissue. We used an analysis protocol developed by NextBio, the details of which have been described previously [20].

cDNA microarray

Expression profiling was generated using the 4 x 44 K whole human genome oligo-microarray ver.2.0 G4845A (Agilent Technologies) as previously described [54]. Raw data were imported into Subio platform ver.1.12 (Subio) for database management and quality control. Raw intensity data were normalized against GAPDH expression levels for further analysis. These raw data have been accepted by GEO (a public repository for microarray data, aimed at storing MIAME). Access to data concerning this study may be found under GEO experiment accession number GSE32886.

Cell lines

All cell lines were cultured at 37°C under the conditions of a humidified atmosphere and 5% CO_2. The human hepatocellular carcinoma-derived Huh7 and human embryonic kidney-derived 293T cells were obtained from Japanese Collection of Research Bioresources (JCRB) Cell Bank (JCRB0403 and JCRB9068), and maintained in DMEM (Sigma) supplemented with 100 U/ml penicillin, 100 μg/ml streptomycin, and 10% fetal calf serum (FCS). The Huh7-derived cell line Huh7.5.1 was kindly provided by F. Chisari. Huh7 cells harboring JFH1-based HCV-SGR were prepared according to the method of a previous report [54] and maintained in DMEM containing 10% FCS and 1 mg/ml G418 (Nakalai Tesque).

Plasmids

The cDNA clones of pri-miR-122, ApoA1, ApoA2, ApoC1, ApoC2, ApoC3, ApoE, ApoH, and AcGFP were inserted between the XhoI and XbaI sites of lentiviral vector pCSII-EF-RfA, which was kindly provided by M. Hijikata, and the resulting plasmids were designated pCSII-EF-miR-122, pCSII-EF-MT-apolipoproteins, and pCSII-EF-AcGFP, respectively. The deletion mutants of ApoC1 and ApoE were amplified by PCR and introduced into pCSII-EF. pHH-JFH1-E2p7NS2mt contains three adaptive mutations in pHH-JFH1 [55]. The pFL-J6/JFH1 plasmid that encodes the entire viral genome of the chimeric strain of HCV-2a, J6/JFH1, was kindly provided by Charles M. Rice [8]. pTH/JFH1 (genotype 1b) and pS310/JFH1 (genotype 3a) were used for the production of chimeric viruses [22,23]. The plasmid pX330, which encodes hCas9 and sgRNA, was obtained from Addgene (Addgene plasmid 42230). The fragments of guided RNA targeting the MTTP gene were inserted into the Bbs1 site of pX330 and designated pX330-MTTP. The plasmids used in this study were confirmed by sequencing with an ABI 3130 genetic analyzer (Life Technologies).

Antibodies

Mouse monoclonal antibodies to HCV core, β-actin and Calnexin were purchased from Thermo Scientific and Sigma Aldrich, respectively. Mouse anti-ApoA1, ApoB, ApoC1, ApoE

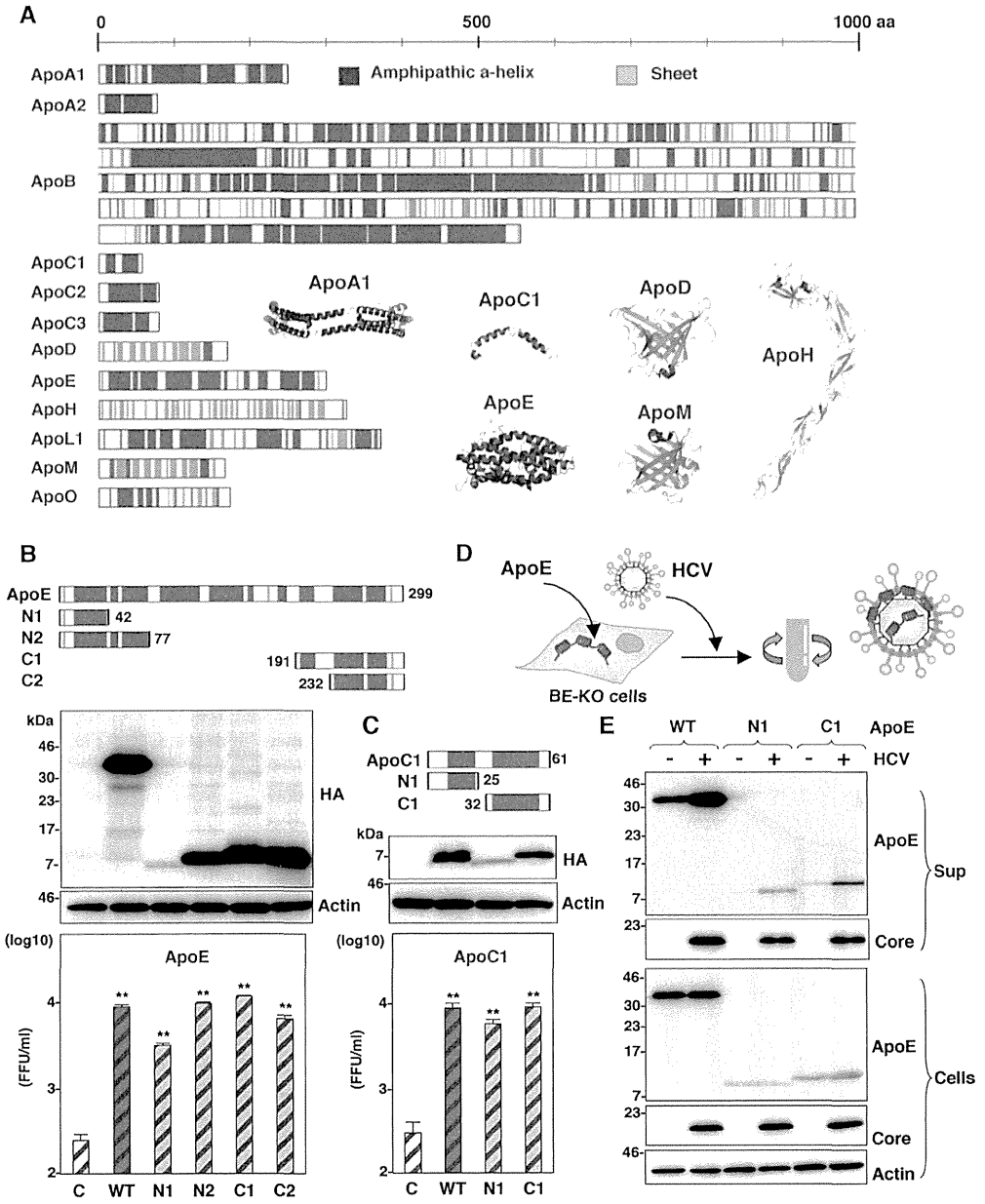

Figure 8. Amphipathic α-helices in apolipoproteins participate in the infectious particle formation of HCV. (A) Predicted or experimentally determined secondary structures of apolipoproteins. Secondary structures of the helices and sheets in the apolipoproteins are colored red and cyan, respectively. The three-dimensional structures of ApoA1 (Protein Data Bank (PDB) ID, 3R2P), ApoC1 (PDB ID, 1IOJ), ApoD (PDB ID, 2HZR), ApoE (PDB ID, 2L7B), ApoH (PDB ID, 1C1Z) and ApoM (PDB ID, 2XKL) are also shown in a ribbon model using the same color code of secondary structures. In cases in which the structure was not available, the secondary structure was predicted by using a CLC Genomics Workbench. (B,C) Schematics of the ApoE- and ApoC1-deletion mutants (upper). Deletion mutants with HA tags expressed in BE-KO1 cells by lentiviral vectors were detected by immunoblotting (middle). BE-KO1 cells expressing the WT or deletion mutants of ApoE or ApoC1 were infected with HCVcc at an MOI of 1, and infectious titers in the culture supernatants were determined by focus-forming assay at 72 h post-infection. Asterisks indicate significant differences (**, $P<0.01$) versus the results for control cells. (D) Schematic of the concentration of viral particles from HCV-infected cells using ultracentrifugation. (E) BE-KO1 cells expressing the WT or deletion mutants of ApoE were infected with HCVcc at an MOI of 1. Culture supernatants harvested at 72 h post-infection were concentrated by ultracentrifugation at 32,000 rpm for 2 h at 4°C, and subjected to immunoblotting.
doi:10.1371/journal.ppat.1004534.g008

and ApoH antibodies were purchased from Cell Signaling, ALerCHEK Inc., Abnova, NOVUS Biologicals, and Santa Cruz Biotechnology, respectively. Rat anti-ApoA2 and Sheep anti-ApoC2 antibodies were purchased from R&D systems. Rabbit anti-NS5A antibody was prepared as described previously [54]. Alexa Fluor (AF) 488-conjugated anti-rabbit or mouse IgG antibodies, and AF594-conjugated anti-mouse IgG2a antibodies were purchased from Life Technologies.

Gene silencing

A small interfering RNA (siRNA) pool targeting various apolipoproteins (siGENOME SMARTpool) and control nontar-

geting siRNA were purchased from Dharmacon, and transfected into cells using Lipofectamine RNAi MAX (Life Technologies) according to the manufacturer's protocol. A human shRNA library was purchased from Takara Bio Inc.

Preparation of viruses

Upon transfection of pHH-JFH1-E2p7NS2mt or *in vitro* transcribed TH/JFH1, J6/JFH1 and S310/JFH1 RNA into Huh7.5.1 cells, HCV in the supernatant was collected after serial passages, and infectious titers were determined by a focus-forming assay and expressed in focus-forming units (FFU) [22,23,54]. To compare the localization of core protein, J6/JFH1 was used in Fig. 6E. Pseudoparticles expressing HCV envelope glycoprotein were generated in 293T cells as previously reported [5], and infectivity was assessed by luciferase expression using the Bright-Glo Luciferase assay system (Promega) and expressed in relative light units (RLU).

Lipofection and lentiviral gene transduction

The lentiviral vectors and ViraPower Lentiviral Packaging Mix (Life Technologies) were co-transfected into 293T cells by Trans IT LT-1 (Mirus), and the supernatants were recovered at 48 h post-transfection. The lentivirus titer was determined by the Lenti-XTM qRT-PCR Titration Kit (Clontech), and the expression levels and AcGFP were determined at 48 h post-inoculation.

Immunoblotting

Cells lysed on ice in lysis buffer (20 mM Tris-HCl [pH 7.4], 135 mM NaCl, 1% Triton-X 100, 10% glycerol) supplemented with a protease inhibitor mix (Nacalai Tesque) were boiled in loading buffer and subjected to 5–20% gradient SDS-PAGE. The proteins were transferred to polyvinylidene difluoride membranes (Millipore) and reacted with the appropriate antibodies. The immune complexes were visualized with SuperSignal West Femto Substrate (Pierce) and detected by the LAS-3000 image analyzer system (Fujifilm).

Generation of gene-knockout Huh7 cell lines

Custom ZFN plasmids were designed to bind and cleave the ApoB, ApoE and MTTP genes and were obtained from Sigma Aldrich. Huh7 cells were transfected with *in vitro* transcribed ZFNs mRNA or pX330-MTTP by Lipofectamine 2000 (Life Technologies), and single cell clones were established by the single cell isolation technique. To screen for gene-knockout Huh7 cell clones, mutations in target loci were determined by using a Surveyor assay as previously described [56]. Frameshift of the genes and deficiencies of protein expression were confirmed by direct sequencing and immunoblotting analysis, respectively.

Enzyme-linked immunosorbent assay (ELISA)

Protein concentrations of ApoB or ApoE in the culture supernatants were determined by using ELISA immunoassay kits (Alercheck Inc.) according to the manufacturer's protocol.

Quantitative RT-PCR

Total RNA was extracted from cells by using an RNeasy minikit (Qiagen) and the first-strand cDNA synthesis and qRT-PCR were performed with TaqMan EZ RT-PCR core reagents and a ViiA7 system (Life Technologies), respectively, according to the manufacturer's protocol. The primers for TaqMan PCR targeted to the noncoding region of HCV RNA were synthesized as previously reported [54]. Taqman Gene expression assays were used as the primers and probes targeting to apolipoproteins (Life Technologies). Fluorescent signals were analyzed with the ViiA7 system.

Immunofluorescence assay

Cells cultured on glass slides were fixed with 4% paraformaldehyde (PFA) in phosphate buffered saline (PBS) at room temperature for 30 min, permeabilized for 20 min at room temperature with PBS containing 0.2% Triton after being washed three times with PBS, and blocked with PBS containing 2% FCS for 1 h at room temperature. The cells were incubated with PBS containing the appropriate primary antibodies at room temperature for 1 h, washed three times with PBS, and incubated with PBS containing AF488- or AF594-conjugated secondary antibodies at room temperature for 1 h. For lipid-droplet staining, cells incubated in medium containing 20 μg/ml BODIPY for 20 min at 37°C were washed with pre-warmed fresh medium and incubated for 20 min at 37°C. Cell nuclei were stained with DAPI. Cells were observed with a FluoView FV1000 laser scanning confocal microscope (Olympus).

In vitro transcription, RNA transfection, and colony formation

The plasmid pSGR-JFH1 was linearized with XbaI, and treated with mung bean exonuclease. The linearized DNA was transcribed *in vitro* by using the MEGAscript T7 kit (Life Technologies) according to the manufacturer's protocol. The *in vitro* transcribed RNA (10 μg) was electroporated into Huh7 cells at 10^7 cells/0.4 ml under conditions of 190 V and 975 μF using a Gene Pulser (Bio-Rad) and plated on DMEM containing 10% FCS. The medium was replaced with fresh DMEM containing 10% FCS and 1 mg/ml G418 at 24 h post-transfection. The remaining colonies were cloned by using a cloning ring (Asahi Glass) or fixed with 4% PFA and stained with crystal violet at 4 weeks post-electroporation.

Intracellular infectivity

Intracellular viral titers were determined according to a method previously reported [10]. Briefly, cells were extensively washed with PBS, scraped, and centrifuged for 5 min at 1000× *g*. Cell pellets were resuspended in 500 μl of DMEM containing 10% FCS and subjected to three cycles of freezing and thawing using liquid nitrogen and a thermo block set to 37°C. Cell lysates were centrifuged at 10,000× *g* for 10 min at 4°C to remove cell debris. Cell-associated infectivity was determined by a focus-forming assay.

Electron microscopy and correlative FM-EM analysis

Correlative fluorescence microscopy-electron microscopy (FM-EM) allows individual cells to be examined both in an overview with fluorescence microscopy and in a detailed subcellular-structure view with electron microscopy. Cells infected with HCVcc were examined by the correlative FM-EM method as described previously [57].

Buoyant density fractionation

Culture supernatants of cells infected with HCVcc were concentrated 50 times by using Spin-X UF concentrators (Corning), and the intracellular proteins collected after freeze-and-thaw were applied to the top of a linear gradient formed from 10–40% OptiPrep (Axis-Shield) in PBS and spun at 32,000 rpm for 16 h at 4°C by using an SW41 Ti rotor (Beckman Coulter). Aliquots of 10 consecutive fractions were collected, and the infectious titer and density were determined.

Proteinase K digestion protection assay

The proteinase K digestion protection assay was performed as described previously [37]. Briefly, cells were extensively washed with PBS, scraped, and centrifuged for 5 min at 1000× *g*. The cell pellets were resuspended in 500 μl of PBS and subjected to three cycles of freezing and thawing using liquid nitrogen and a thermo block set to 37°C. The cell lysates were centrifuged at 10,000× *g* for 10 min at 4°C to remove cell debris. The cell lysates were then incubated with 50 μg/ml proteinase K (Life Technologies) in the presence or absence of 5% Triton-X for 1 h on ice, and the digestion was terminated by addition of PMSF (Wako Chemical Industries).

Statistics

The data for statistical analyses are the average of three independent experiments. Results were expressed as the means ± standard deviation. The significance of differences in the means was determined by Student's *t*-test.

Supporting Information

Figure S1 Establishment of ApoB- or ApoE-knockout Huh7 cell lines. Target sequences of ZFNs to ApoB (A) and ApoE (B) are indicated by red characters inside a red box at the top of the panel. Gene knockout by the sequence modification in the 2 alleles of the ApoB (A) or ApoE (B) gene in knockout cell lines (B-KO1 and B-KO2, or E-KO1 and E-KO2) is shown. Deletion and insertion of the sequences are indicated by dotted lines and blue characters in brackets, respectively. Absence of the expressions of ApoB (C) and ApoE (D) in the knockout cell lines was confirmed by immunoblotting using anti-ApoB and -ApoE antibodies. Expression of ApoB (E) and ApoE (F) in the culture supernatants of 293T, Huh7 and the knockout cell lines was determined by ELISA.
(TIF)

Figure S2 Both ApoB and ApoE are involved in the formation of infectious HCV particles. (A) HCVpp were inoculated into Huh7, B-KO1, B-KO2, E-KO1 and E-KO2 cells, and luciferase activities were determined at 48 h post-infection. (B) A subgenomic HCV RNA replicon of the JFH1 strain was electroporated into Huh7, B-KO1 and E-KO1 cells, and colonies were stained with crystal violet at 31 days post-electroporation after selection with 400 μg/ml of G418. HCVcc were inoculated into Huh7, B-KO1, B-KO2, E-KO1 and E-KO2 cells at an MOI of 1 and intracellular HCV RNA at 12, 24, 36 and 60 h post-infection (C), and infectious titers in the culture supernatants at 72 h post-infection (D) were determined by qRT-PCR and focus-forming assay, respectively. (E) Exogenous expression of ApoE in E-KO1 and E-KO2 cells by lentiviral vector was determined by immunoblotting analysis (upper), and infectious titers in the culture supernatants of cells infected with HCVcc at an MOI of 1 were determined at 72 h post-infection by focus-forming assay (lower).
(TIF)

Figure S3 Establishment of ApoB and ApoE double-knockout (BE-KO) Huh7 cell lines. Gene knockout by the ZFN in the 2 alleles of the ApoB and ApoE genes in the double-knockout cell lines, BE-KO1 (A) and BE-KO2 (B), is shown. Deletion and insertion of the sequences are indicated by dotted lines and blue characters in brackets, respectively. (C) The absence of the expressions of ApoB and ApoE in BE-KO1 and BE-KO2 was confirmed by immunoblotting using anti-ApoB and -ApoE antibodies. Expression of ApoB (D) and ApoE (E) in the culture supernatants of 293T, Huh7, BE-KO1 and BE-KO2 cells was determined by ELISA.
(TIF)

Figure S4 Establishment of MTTP-knockout (M-KO) and ApoE and MTTP double-knockout (EM-KO) Huh7 cell lines. (A) Gene knockout by the ZFN in the 2 alleles of the MTTP gene in the knockout cell lines, M-KO1 and M-KO2, is shown. (B) Expression of MTTP in Huh7, M-KO1 and M-KO2 cells was determined by immunoblotting. Expression of ApoB (C) and ApoE (D) in the culture supernatants of Huh7, M-KO1, M-KO2 and 293T cells was determined by ELISA. (E) Gene knockout in the 2 alleles of the MTTP genes by the CRISPR/Cas9 system and in one allele of the ApoE gene by the ZFN in the double-knockout cell lines, EM-KO1 and EM-KO2, is shown. (F) Expression of MTTP in Huh7, EM-KO1 and EM-KO2 cells was determined by immunoblotting. Expression of ApoB (G) and ApoE (H) in the culture supernatants of Huh7, EM-KO1, EM-KO2 and 293T cells was determined by ELISA. (I) Expression of ApoB mRNA in Huh7, M-KO1, M-KO2, EM-KO1, EM-KO2 and 293T cells was determined by qRT-PCR.
(TIF)

Figure S5 Gene silencing of apolipoproteins. BE-KO1 cells infected with HCVcc at an MOI of 1 at 6 h post-transfection with siRNAs targeting ApoA1, ApoA2, ApoC1, ApoC2, ApoC3 and ApoH, and the expression levels of these apolipoproteins were determined by q-RT PCR using specific primers and probes.
(TIF)

Figure S6 ApoD, ApoL1, and ApoO do not participate in the formation of infectious HCV particles. Exogenous expression of ApoD, ApoE, ApoL1 and ApoO in BE-KO1 cells by lentiviral vector was determined by immunoblotting analysis (upper), and infectious titers in the culture supernatants of cells infected with HCVcc at an MOI of 1 were determined at 72 h post-infection by focus-forming assay (lower).
(TIF)

Figure S7 BE-KO1 cells permit propagation of JEV and DENV. Huh7, BE-KO1 and ApoE-restored (ApoE-res) cells were infected with JEV and DENV at an MOI of 0.1, and infectious titers in the culture supernatants were determined by focus-forming assay at 48 h post-infection.
(TIF)

Figure S8 Localization of core, NS5A proteins and ER in BE-KO Huh7 cells. BE-KO1 cells infected with HCVcc at an MOI of 1 were subjected to immunofluorescence analyses by using antibodies against core, NS5A and Calnexin.
(TIF)

Acknowledgments

We thank M. Tomiyama for her secretarial work and M. Ishibashi and Y. Sugiyama for their technical assistance. We also thank M. Hijikata, T. Wakita, R. Bartenschlager, F. Chisari, and M. Whitt for providing experimental materials.

Author Contributions

Conceived and designed the experiments: TF SN MY IS TW KK YM. Performed the experiments: TF MW CO MS SY TM. Analyzed the data: TF MW SN TO DO YM. Contributed reagents/materials/analysis tools: KK YM. Wrote the paper: TF SN DO YM.

References

1. Maasoumy B, Wedemeyer H (2012) Natural history of acute and chronic hepatitis C. Best. Pract. Res. Clin. 26: 410–412.
2. Jacobson IM, McHutchison JG, Dusheiko G, Di Bisceglie AM, Reddy KR, et al. (2011) Telaprevir for previously untreated chronic hepatitis C virus infection. N. Engl. J. Med. 364: 2405–2416.
3. Sulkowski MS, Gardiner DF, Rodriguez-Torres M, Reddy KR, Hassanein T, et al. (2014) Daclatasvir plus Sofosbuvir for previously treated or untreated chronic HCV infection. N. Engl. J. Med. 370: 211–221.
4. Janssen HL, Reesink HW, Lawitz EJ, Zeuzem S, Rodriguez-Torres M, et al. (2013) Treatment of HCV infection by targeting microRNA. N. Engl. J. Med. 368: 1685–1694.
5. Bartosch B, Dubuisson J, Cosset F (2003) Infectious hepatitis C virus pseudo-particles containing functional E1–E2 envelope protein complexes. J. Exp. Med. 197: 633–642.
6. Lohmann V, Korner F, Koch JO, Herian U, Theilmann L, et al. (1999) Replication of subgenomic hepatitis C virus RNAs in a hepatoma cell line. Science. 285: 110–113.
7. Wakita T, Pietschmann T, Kato T, Date T, Miyamoto M, et al. (2005) Production of infectious hepatitis C virus in tissue culture from a cloned viral genome. Nat. Med. 11: 791–796.
8. Lindenbach BD, Evans MJ, Syder AJ, Wolk B, Tellinghuisen TL, et al. (2005) Complete replication of hepatitis C virus in cell culture. Science. 309: 623–626.
9. Jirasko V, Montserret R, Lee JY, Gouttenoire J, Moradpour D, et al. (2010) Structural and functional studies of nonstructural protein 2 of the hepatitis C virus reveal its key role as organizer of virion assembly. PLoS Pathog. 6: e1001233.
10. Gastaminza P, Cheng G, Wieland S, Zhong J, Liao W, et al. (2008) Cellular determinants of hepatitis C virus assembly, maturation, degradation, and secretion. J. Virol. 82: 2120–2129.
11. Jiang J, Luo G (2009) Apolipoprotein E but not B is required for the formation of infectious hepatitis C virus particles. J. Virol. 83: 12680–12691.
12. Andre P, Komurian-Pradel F, Deforges S, Perret M, Berland L, et al. (2002) Characterization of Low- and Very-Low-Density hepatitis C virus RNA-containing particles. J. Virol. 76: 6919–6928.
13. Saito H, Lund-Katz S, Phillips MC. (2004) Contribution of domain structure and lipid interaction to the functionality of exchangeable human apolipoproteins. Prog. Lipid Res. 43: 350–380.
14. Narayanaswami V, Kiss RS, Weers PM. (2010) The helix bundle: A reversible lipid binding motif. Comp. Biochem. Physiol. A Mol. Integr. Physiol. 155: 123–133.
15. Mancone C, Steindler C, Santangelo L, Simonte G, Vlassi C, et al. (2011) Hepatitis C virus production requires apolipoprotein A-1 and affects its association with nascent low-density lipoproteins. Gut. 60: 378–386.
16. Da Costa D, Turek M, Felmee DJ, Girardi E, Pfeffer S, et al. (2012) Reconstitution of the entire hepatitis C virus life cycle in nonhepatic cells. J. Virol. 86: 11919–11925.
17. Porteus MH, Carroll D (2005) Gene targeting using zinc finger nucleases. Nat. Biotechnol. 23: 967–973.
18. Zhang F, Cong L, Lodato S, Kosuri S, Church GM, et al. (2011) Efficient construction of sequence-specific TAL effectors for modulating mammalian transcription. Nat. Biotechnol. 29: 149–153.
19. Mali P, Yang L, Esvelt KM, Aach J, Guell M, et al. (2013) RNA-guided human genome engineering via Cas9. Science. 339: 823–826.
20. Kupershmidt I, Su QJ, Grewal A, Sundaresh S, Halperin I, et al. (2010) Ontology-based meta-analysis of global collections of high-throughput public data. PLoS One. 5: e13066.
21. Hussain MM, Shi J, Dreizen P (2003) Microsomal triglyceride transfer protein and its role in apoB-lipoprotein assembly. J. Lipid Res. 44: 22–32.
22. Takebe Y, Saucedo CJ, Lund G, Uenishi R, Hase S, et al. (2013) Antiviral lectins from Red and Blue-Green Algae show potent *in vitro* and *in vivo* activity against hepatitis C virus. PLoS One. 8: e64449.
23. Kim S, Date T, Yokokawa H, Kono T, Aizaki H, et al. (2014) Development of hepatitis C virus genotype 3a cell culture system. Hepatology. doi: 10.1002/hep.27197.
24. Miyanari Y, Atsuzawa K, Usuda N, Watashi K, Hishiki T, et al. (2007) The lipid droplet is an important organelle for hepatitis C virus production. Nat. Cell Biol. 9: 961–969.
25. Boson B, Granio O, Bartenschlager R, Cosset F (2011) A concerted action of hepatitis C virus p7 and nonstructural protein 2 regulates core localization at the endoplasmic reticulum and virus assembly. PLoS Pathog. 7: e1002144.
26. Gentzsch J, Brohm C, Steinmann E, Friesland M, Menzel N, et al. (2013) Hepatitis C virus p7 is critical for capsid assembly and envelopment. PLoS Pathog. 9: e1003355.
27. Shavinskaya A, Boulant S, Penin F, McLauchlan J, Bartenschlager R. (2007) The lipid droplet binding domain of hepatitis C virus core protein is a major determinant for efficient virus assembly. J. Biol. Chem. 282: 37158–37169.
28. Ai L, Lee Y, Chen SS (2009) Characterization of hepatitis C virus core protein multimerization and membrane envelopment: revelation of a cascade of core-membrane interactions. J. Virol. 83: 9923–9939.
29. Mei X, Atkinson D (2011) Crystal structure of C-terminal truncated apolipoprotein A-1 reveals the assembly of high density lipoprotein (HDL) by dimerization. J. Biol. Chem. 286: 38570–38582.
30. Rozek A, Sparrow JT, Weisgraber KH, Cushley JR (1999) Conformation of human apolipoprotein C-1 in a lipid-mimetic environment determined by CD and NMR spectrometry. Biochemistry. 38: 14475–14484.
31. Eichinger A, Nasreen A, Jin H (2007) Structural insight into the dual ligand specificity and mode of high density lipoprotein association of apolipoprotein D. J. Biol. Chem. 282: 31068–31075.
32. Chen J, Li Q, Wang J (2011) Topology of human apolipoprotein E3 uniquely regulates its diverse biological functions. Proc. Natl. Acad. Sci. U. S. A. 108: 14813–14818.
33. Schwarzenbacher R, Zeth K, Diederichs K, Gries A, Kostner GM, et al. (1999) Crystal structure of human β2-glycoprotein 1: implication for phospholipid binding and the antiphospholipid syndrome. EMBO J. 18: 6228–6239.
34. Sevvana M, Kassler K, Ahnstrom J, Weiler S, Dahlback B, et al. (2010) Mouse ApoM displays an unprecedented seven-stranded lipocalin fold: folding decoy or alternative native fold? J. Mol. Biol. 404: 363–371.
35. Nielsen SU, Bassendine MF, Burt AD, Martin C, Pumeechockchai W, et al. (2006) Association between hepatitis C virus and very-low-density lipoprotein (VLDL)/LDL analyzed in iodixanol density gradients. J. Virol. 80: 2418–2428.
36. Jammart B, Michelet M, Pecheur E, Parent R, Bartosch B, et al. (2013) Very-low-density lipoprotein (VLDL)-prpducing and hepatitis C virus-replicating HepG2 cells secrete no more lipoviroparticles than VLDL-deficient Huh7.5 cells. J. Virol. 87: 1405–1412.
37. Hueging K, Doepke M, Vieyres G, Bankwitz D, Frentzen A, et al. (2014) Apolipoprotein E codetermines tissue tropism of hepatitis C virus and is crucial for viral cell-to-cell transmission by contributing to a postenvelopment step of assembly. J. Virol. 88: 1433–1466.
38. Coller KE, Heaton NS, Berger KL, Cooper JD, Saunders JL, et al. (2012) Molecular determinants and dynamics of hepatitis C virus secretion. PLoS Pathog. 8: e1002466.
39. Catanese TM, Uryu K, Kopp M, Edwards TJ, Andrus L, et al. (2013) Ultrastructural analysis of hepatitis C virus particles. Proc. Natl. Acad. Sci. U. S. A. 110: 9505–9510.
40. Cheng G, Montero A, Gastaminza P, Whitten-Bauer C, Wieland SF, et al. (2008) A virocidal amphipathic α-helical peptide that inhibits hepatitis C virus infection *in vitro*. Proc. Natl. Acad. Sci. U. S. A. 105: 3088–3093.
41. Scarselli E, Ansuini H, Cerino R, Roccasecca RM, Acali S, et al. (2002) The human scavenger receptor class B type 1 is a novel candidate receptor for the hepatitis C virus. EMBO J. 21: 5017–5025.
42. Molina S, Castet V, Fournier-Wirth C, Pichard-Garcia L, Avner R, et al. (2007) The low-density lipoprotein receptor plays a role in the infection of primary human hepatocytes by hepatitis C virus. J. Hepatol. 46: 411–419.
43. Owen DM, Huang H, Ye J, Gale MJ (2009) Apolipoprotein E on hepatitis C virion facilitates infection through interaction with low-density lipoprotein receptor. Virology. 394: 99–108.
44. Prentoe J, Serre SB, Ramirez S, Nicosia A, Gottwein JM, et al. (2014) Hypervariable region 1 deletion and required adaptive envelope mutations confer decreased dependency on scavenger receptor class B type 1 and low density lipoprotein receptor for hepatitis C virus. J. Virol. 88: 1725–1739.
45. Meunier J, Russell RS, Engle RE, Faulk KN, Purcell RH, et al. (2008) Apolipoprotein C1 association with hepatitis C virus. J. Virol. 82: 9647–9656.
46. Dreux M, Boson B, Ricard-Blum S, Molle J, Lavillette D et al. (2007) The exchangeable apolipoprotein ApoC-1 promotes membrane fusion of hepatitis C virus. J. Biol. Chem. 282: 32357–32369.
47. Fukuhara T, Matsuura Y (2013) Role of miR-122 and lipid metabolism in HCV infection. J. Gastroenterol. 48: 169–176.
48. Ploss A, Evans MJ, Gaysinskaya VA, Panis M, You H, et al. (2009) Human occludin is a hepatitis C virus entry factor required for infection of mouse cells. Nature. 457: 882–886.
49. Mercer DF, Schiller DE, Elliott JF, Douglas DN, Hao C, et al. (2001) Hepatitis C virus replication in mice with chimeric human livers. Nat. Med. 7: 927–933.
50. Dorner M, Horwitz JA, Donovan BM, Labitt RN, Budell BC, et al. (2013) Completion of the entire hepatitis C virus life cycle in genetically humanized mice. Nature. 501: 237–241.
51. Wang H, Yang H, Shivalila CS, Dawlaty MM, Cheng AW, et al. (2013) One-step generation of mice carrying mutations in multiple genes by CRISPR/Cas-mediated genome engineering. Cell. 153: 910–918.
52. Cho SW, Kim S, Kim JM, Kim J (2013) Targeted genome engineering in human cells with the Cas9 RNA-guided endonuclease. Nat. Biotechnol. 31: 230–232.
53. Shalem O, Sanjana NE, Hartenian E, Shi X, Scott DA, et al. (2014) Genome-scale CRISPR-Cas9 knockout screening in human cells. Science. 343: 84–87.
54. Fukuhara T, Kambara H, Shiokawa M, Ono C, Katoh H, et al. (2012) Expression of microRNA miR-122 facilitates an efficient replication in nonhepatic cells upon infection with hepatitis C virus. J. Virol. 86: 7918–7933.
55. Russell RS, Meunier JC, Takikawa S, Faulk K, Engle RE, et al. Advantages of a single-cycle production assay to study cell culture-adaptive mutations of hepatitis C virus. Proc. Natl. Acad. Sci. U. S. A. 105: 4370–4375 (2008).
56. Guschin YD, Waite AJ, Katibah GE, Miller JC, Holmes MC, et al. (2010) A rapid and general assay for monitoring endogenous gene modification. Methods Mol. Biol. 649: 247–256 (2010).
57. Rieder CL, Bowser SS (1985). Correlative immunofluorescence and electron microscopy on the same section of epon-embedded material. J. Histochem. Cytochem. 33: 165–171.

Published online: March 25, 2014

Scientific Report

SOURCE DATA TRANSPARENT PROCESS

EMBO reports

Structural determinants in GABARAP required for the selective binding and recruitment of ALFY to LC3B-positive structures

Alf Håkon Lystad[1], Yoshinobu Ichimura[2], Kenji Takagi[3], Yinjie Yang[2], Serhiy Pankiv[1], Yumi Kanegae[4], Shun Kageyama[2], Mariko Suzuki[4], Izumu Saito[4], Tsunehiro Mizushima[3], Masaaki Komatsu[2,**] & Anne Simonsen[1,*]

Abstract

Several autophagy proteins contain an LC3-interacting region (LIR) responsible for their interaction with Atg8 homolog proteins. Here, we show that ALFY binds selectively to LC3C and the GABARAPs through a LIR in its WD40 domain. Binding of ALFY to GABARAP is indispensable for its recruitment to LC3B-positive structures and, thus, for the clearance of certain p62 structures by autophagy. In addition, the crystal structure of the GABARAP-ALFY-LIR peptide complex identifies three conserved residues in the GABARAPs that are responsible for binding to ALFY. Interestingly, introduction of these residues in LC3B is sufficient to enable its interaction with ALFY, indicating that residues outside the LIR-binding hydrophobic pockets confer specificity to the interactions with Atg8 homolog proteins.

Keywords ALFY; GABARAP; LC3; LIR; structure
Subject Categories Autophagy & Cell Death; Membrane & Intracellular Transport; Structural Biology
DOI 10.1002/embr.201338003 | Received 24 September 2013 | Revised 21 February 2014 | Accepted 24 February 2014 | Published online 25 March 2014
EMBO Reports (2014) 15: 557–565

Introduction

Sequestration of cytoplasmic cargo for degradation by macroautophagy (hereafter autophagy) is facilitated by binding of cargo-interacting proteins, so-called autophagy receptors, to Atg8-homolog proteins, which upon the induction of autophagy becomes covalently linked to phosphatidylethanolamine (PE) in the autophagic membrane [1]. Whereas yeast has a single *Atg8* gene, mammals have seven Atg8 homologs, which can be divided into two subfamilies: the LC3 family (including LC3A, LC3B, LC3B2 and LC3C) and the GABARAP family (including GABARAP, GABARAPL1 and GABARAPL2) [2]. The reason for such an expansion of this protein family in higher eukaryotes is unclear, but it coincides with the expansion of cargo-recognition proteins and is likely to provide specificity to cargo recruitment.

The currently known autophagy receptors include receptors for the recognition of bacteria, viral particles, mitochondria, peroxisomes, midbody remnants and protein aggregates [1]. They generally interact with two hydrophobic pockets in the Atg8 proteins through a linear motif called an LC3-interacting region (LIR), having the consensus sequence [W/F/Y]-x-x-[I/L/V][1]. Whereas some autophagy receptors seem to interact with all Atg8 proteins *in vitro*, others show selective binding to a few Atg8 family members. The structural determinants in Atg8 proteins responsible for such selectivity remain to be determined in most cases, but it was recently shown that the specific interaction of the autophagy receptor NDP52 with LC3C requires, in addition to its noncanonical LIR motif xLVV (termed a CLIR), interactions outside the CLIR-binding pocket [3].

ALFY (autophagy-linked FYVE protein, also called WDFY3) is a large phosphatidyl-inositol 3-phosphate-binding protein shown to be recruited to ubiquitin-positive structures during stress. ALFY interacts with the ubiquitin-binding autophagy receptors p62/SQSTM1 and NBR1 [4,5] and contributes to autophagic clearance of aggregated proteins [5]. In this study, we show that ALFY binds selectively to the GABARAP subfamily, and weakly to LC3C, through a conserved LIR motif in its WD40 region. We demonstrate that the interaction of ALFY with GABARAPs is indispensable for the recruitment of LC3B to ALFY-p62-positive structures. We further identify three conserved residues in the GABARAPs that confer selectivity to the interaction with ALFY and show that introduction of these residues in the corresponding positions of LC3B is sufficient to enable interaction of ALFY with LC3B.

1 Institute of Basic Medical Sciences, University of Oslo, Oslo, Norway
2 Protein Metabolism Project, Tokyo Metropolitan Institute of Medical Science, Tokyo, Japan
3 Picobiology Institute, Graduate School of Life Science, University of Hyogo, Hyogo, Japan
4 Laboratory of Molecular Genetics, Institute of Medical Science, University of Tokyo, Tokyo, Japan
*Corresponding author. Tel: +47 22851110; Fax: +47 22851058; E-mail: anne.simonsen@medisin.uio.no
**Corresponding author. Tel: +81 3 5316 3244; Fax: +81 3 5316 3152; E-mail: komatsu-ms@igakuken.or.jp

Results and Discussion

ALFY interacts selectively and directly with LC3C and GABARAP family proteins

ALFY was identified in a proteomic approach aimed at finding new GABARAP-interacting proteins (Unpublished observations). In order to verify this interaction, cells were transfected with GFP-tagged Atg8 homologs of the LC3 and GABARAP subfamilies, followed by anti-GFP immunoprecipitation (IP) and immunoblotting for endogenous ALFY (Fig 1A). Whereas there was little or no interaction between ALFY and LC3A or LC3B, ALFY was found to co-IP with GABARAP, GABARAPL1 and GABARAPL2, but also weakly with LC3C (Fig 1A).

To determine the minimal region of ALFY required for its interaction with GABARAP, we initially performed GST pull-down assays with *in vitro*-translated GFP-ALFY constructs that covered its entire cDNA sequence (Fig 1B). The C-terminal part of ALFY was found to interact strongly with GABARAP, and the binding site was mapped to amino acid (aa) 3313–3363, located between the fourth and fifth WD40 repeat of ALFY (Fig 1B, C). This part of ALFY was also sufficient to co-IP endogenous GABARAP when transfected into HEK293T cells (Supplementary Fig S1A, B). The interaction between ALFY and GABARAPs was shown to be direct, as recombinant ALFY (aa 2981–3526) was efficiently pulled down with GST-GABARAPs and weakly with GST-LC3C (Fig 1D). These results indicate that ALFY selectively and directly interacts with LC3C and GABARAP family proteins.

Identification of a LIR in ALFY

When aligning the $ALFY_{3313–3363}$ sequence with the LIR consensus motif [W/F/Y]-x-x-[I/L/V], we found one perfect alignment, F-I-F-V (aa 3346–3349), that was conserved in homologous ALFY sequences (Fig 2A). Mutation of the potential LIR residues F3346, I3347, F3348 or V3349 to Ala/A all caused a large decrease in the binding of *in vitro*-translated GFP-$ALFY_{2981–3526}$ to GABARAP and LC3C (Fig 2B and Supplementary Fig S1C). As the first Phe/F of the core LIR proved essential for the interactions, we propose that binding of ALFY to Atg8 homolog proteins is mediated by a canonical LIR motif. However, as mutation of the I3347 residue had a greater impact on the binding to LC3C than to GABARAP, we cannot exclude the possibility that ALFY has a hybrid LIR/CLIR motif. The importance of this motif was further validated with purified proteins, showing that MBP-$ALFY_{3255–3526}$, but not the LIR mutant ($ALFY_{3255–3526\ F3346A}$), was able to interact directly with GABARAP (Fig 2C). To further investigate the affinity of ALFY for different Atg8 proteins, we performed isothermal titration calorimetry (ITC) (Fig 2D and Supplementary Fig S1D). The ALFY-LIR peptide (aa 3341–3354) used in this assay showed similar binding specificity for Atg8 proteins, with strong affinity to the GABARAP family proteins (0.327–0.871 μM), weak affinity for LC3C (20.8 μM) and no interaction with LC3B. Furthermore, we show that the LIR motif is functionally conserved, as the corresponding LIR peptide from the *Drosophila* ALFY homolog, Blue Cheese [6], bound strongly and specific to purified dAtg8a protein (Fig 2E), in line with dAtg8a being more similar to GABARAPs than LC3s.

Overall structure of the GABARAP-ALFY-LIR complex

Next we decided to determine the structure of the GABARAP-ALFY-LIR complex (PDB ID code 3WIM) by X-ray crystallography (Fig 3A and Supplementary Table S1). The complex consists of full-length GABARAP (aa 1–117) bound to an ALFY-LIR peptide (aa 3341–3354), and its crystal structure was determined by molecular replacement using wild-type GABARAP (PDB ID code 1GNU) and refined to 2.6 Å resolution (Fig. 3A). This represents the first structural determination of GABARAP with a physiological LIR-containing peptide and is essentially identical to the previously reported structures of peptide-free GABARAP [7,8]. The ALFY-LIR-binding surface of GABARAP consists of three linkers (α2-β1, β1-β2 and β2-α3), an α-helix (α2) and two β-strands (β1 and β2). The side chains of the core ALFY-LIR residues (F3346 and V3349) are bound deeply into two hydrophobic pockets of GABARAP (Supplementary Fig S2A and B), similar to that observed between LC3B and the LIR moiety of other LIR-containing proteins, including p62 [9], Atg4B [10] and optineurin [11].

Conserved residues in GABARAP determine the binding specificity of ALFY

To try to understand why ALFY interacts with GABARAP and not with LC3B, we superimposed the LC3B structure (PDB ID code 1UGM) onto the GABARAP-ALFY-LIR structure (Fig 3B). While both LC3B and GABARAP can accommodate the core ALFY-LIR residues (F3346 and V3349), it is clear from this model that D3344 of the ALFY-LIR is able to form ionic interactions with K24 and Y25 of GABARAP, but not with the corresponding Q26 and H27 of LC3B (Fig 3B and Supplementary Fig S2C). Moreover, while D54 of GABARAP can interact with Y3351 of the ALFY-LIR, the corresponding H57 of LC3B causes steric hindrance between the two side chains (Fig 3B and Supplementary Fig S2D). Interestingly, the

Figure 1. The C-terminal region of ALFY interacts with GABARAP.

A Transfected GFP-Atg8 homologs were immunoprecipitated with μMACS™ from total U2OS cell extracts followed by immunoblot analysis with anti-GFP and anti-ALFY antibodies. Data are representative of two independent experiments.

B An overview of the deletion mutant constructs of ALFY used for GST pull-down experiments in (C).

C The indicated ^{35}S-labelled *in vitro*-translated GFP-tagged constructs were incubated with GST, GST-LC3B or GST-GABARAP conjugated to glutathione Sepharose, and their binding was evaluated by autoradiography (ARG). 5% of the *in vitro*-translated protein (arrow head) used was loaded. Equal amounts of GST proteins were used as shown by Coomassie Brilliant Blue (CBB) staining. Data are representative of three independent experiments.

D Recombinant ALFY (aa 2981–3526) was incubated with GST-Atg8 proteins conjugated to glutathione Sepharose. The pulled-down complexes were subjected to SDS–PAGE and anti-ALFY and anti-GST immunoblotting. 5% of the recombinant ALFY protein used was loaded as input. Data are representative of three independent experiments.

Source data are available online for this figure.

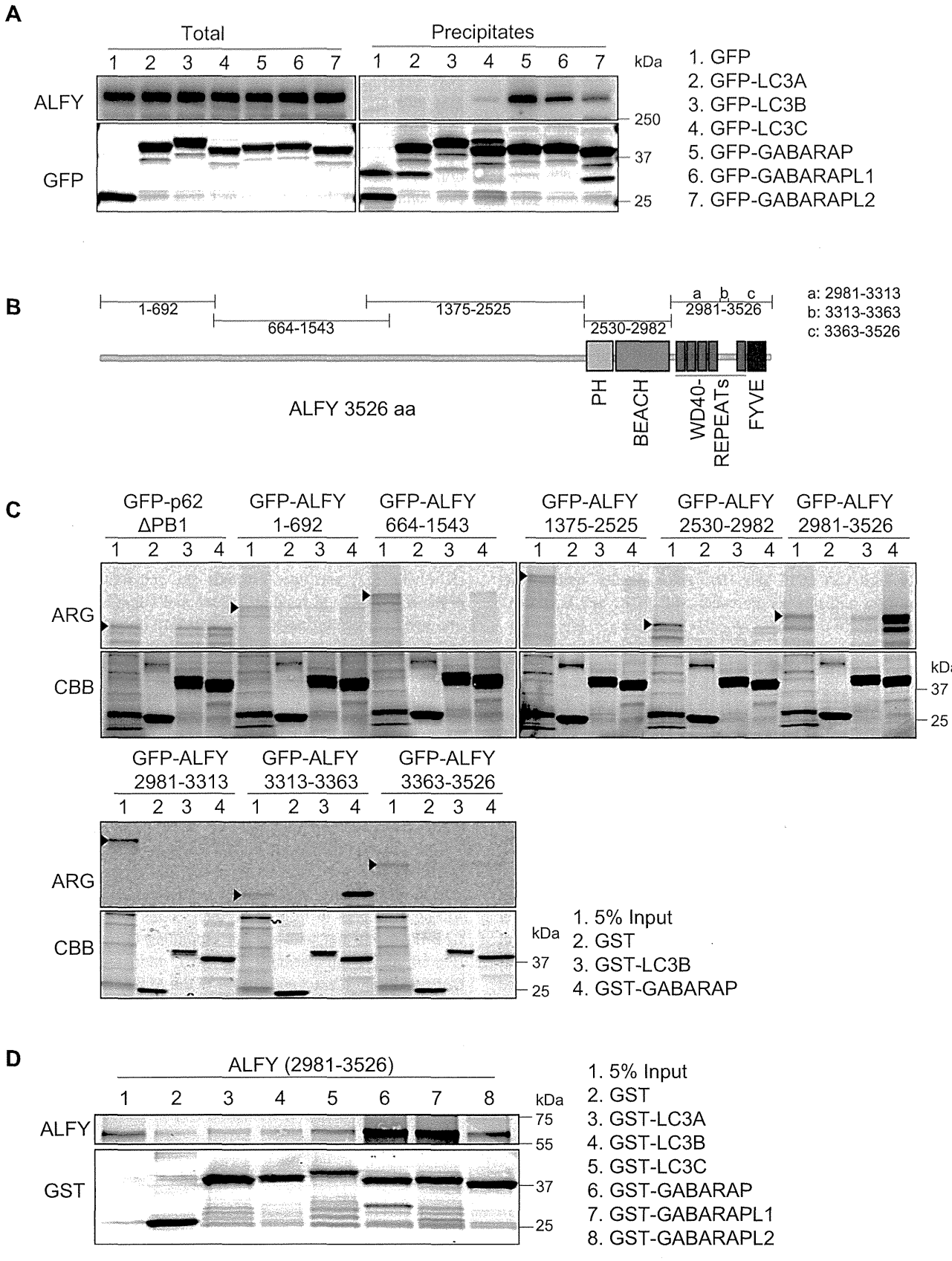

A

B

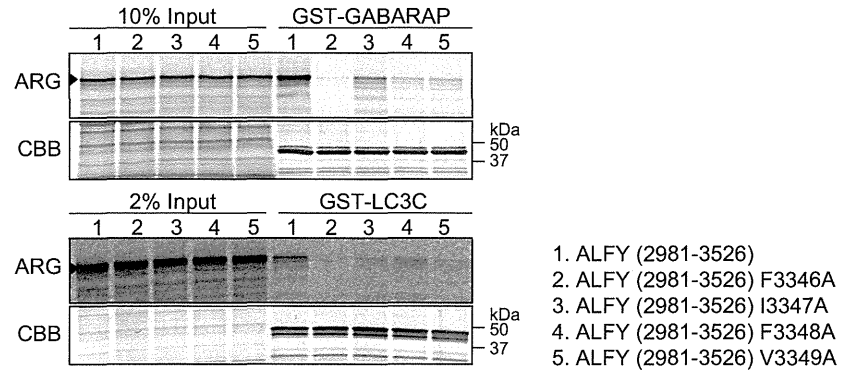

C

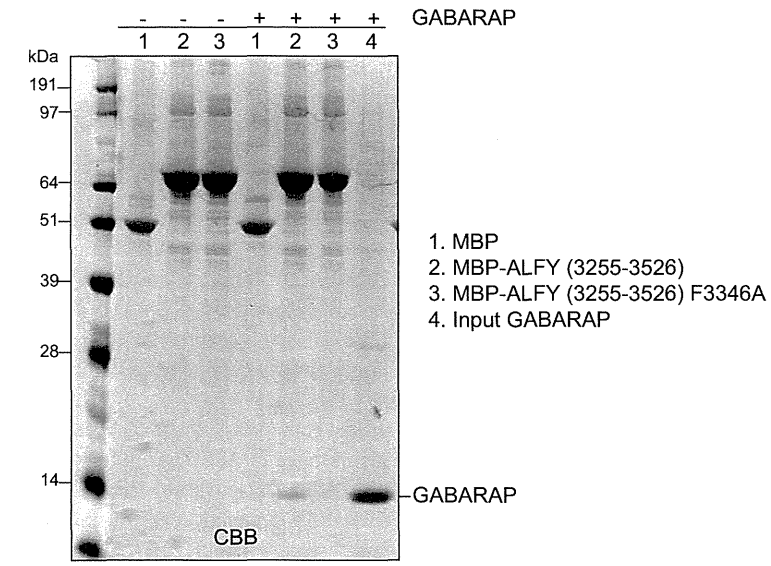

D

PROTEIN	LC3B	LC3C	GABARAP	GABARAPL1	GABARAPL2
K_D (μM)	ND	20.8±3.16	0.327±0.03	0.387±0.021	0.871±0.119
N (sites)	ND	0.87±0.04	0.956±0.003	0.921±0.002	1.06±0.007
ΔH (cal mol^{-1})	ND	-4940±340.9	-7456±45.28	-6818±20.78	-5710±64.15
ΔS (cal mol^{-1} deg^{-1})	ND	4.90	4.69	6.47	8.61

E

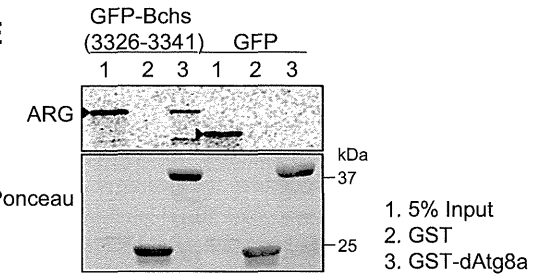

Figure 2. Identification of the LC3-interacting region (LIR) in ALFY.

A Alignment of the potential LIR in human ALFY to the corresponding homolog sequences of representatives of mammals, birds, fish and insects. Ω indicates an aromatic residue, while Ψ indicates an aliphatic residue.

B ^{35}S-labelled *in vitro*-translated GFP-ALFY (aa 2981–3526) wild-type and different LIR mutants were incubated with GST-GABARAP or -LC3C and binding evaluated by ARG. 10 and 2% of the *in vitro*-translated proteins used were loaded to illustrate binding affinity. CBB staining shows equal amounts of GST proteins used. Data are representative of three independent experiments.

C MBP, MBP-ALFY (aa 3255–3526) or the ALFY-LIR mutant (F3346A) conjugated to amylose resins was incubated in the absence or presence of purified GABARAP. The pulled-down complexes were subjected to SDS–PAGE and visualized by CBB staining. Data are representative of three independent experiments.

D Thermodynamic parameters of ALFY-LIR peptide (aa 3341–3354) to Atg8 homologs. All titrations were performed at 25°C as described in Supplementary Methods. ITC data were fitted to a one-site binding model. ND, not detected.

E ^{35}S-labelled *in vitro*-translated GFP or GFP-Bchs (aa 3326–3341) were incubated with GST or GST-dAtg8a and binding evaluated by ARG. 5% of the *in vitro*-translated protein used was loaded. Ponceau staining shows equal amounts of GST proteins used. Data are representative of three independent experiments.

Source data are available online for this figure.

K24/Y25/D54 residues of GABARAP are conserved in GABARAPL1 and GABARAPL2 (Fig 3C), which both bind to ALFY (Figs 1A, D and 2D). Moreover, the corresponding residues in LC3C (K32/F33/E63) are similar to the GABARAP subfamily (Fig 3C) and have been implicated in the specific binding to NDP52 [3]. We therefore speculated that these three residues are responsible for the specific interaction of ALFY with GABARAPs and LC3C. In order to test this experimentally, we substituted these three amino acids in LC3B with the corresponding amino acids of GABARAP and created HeLa cells with stable inducible expression of the triple mutant protein (GFP-LC3B Q26K/H27Y/H57D). When compared to cells expressing wild-type LC3B, we found increased binding of endogenous ALFY to the LC3B triple mutant (Q26K/H27Y/H57D) (Fig 3D). We next substituted these three residues in GABARAP with the corresponding LC3B residues, either individually or combined (Fig 3E, F). While the GABARAP single mutants had little or no effect on the interaction with ALFY, the triple GABARAP mutant (K24Q/Y25H/D54H) was significantly compromised in the ability to bind to MBP-ALFY$_{3255–3526}$ (Fig 3E, F and Supplementary Fig S2E). Moreover, in line with our result in Fig 3D, recombinant protein of the LC3B triple mutant (Q26K/H27Y/H57D) showed a strong and LIR-dependent interaction with MBP-ALFY$_{3255–3526}$ (Fig 3F). In contrast, the interaction between p62 and GABARAP/LC3B proteins was not affected to the same degree by mutation of these residues, as both the LC3B triple mutant (Q26K/H27Y/H57D) and the GABARAP triple mutant (K24Q/Y25H/D54H) bound to MBP-p62$_{168–391}$ with similar affinity as to wild-type GABARAP/LC3B proteins (Fig 3F). To test whether the ALFY-LIR residues involved in interactions with GABARAP K24/Y25/D54 were equally required for the specificity of the interaction, these residues (K3343/D3344/Y3351) were mutated in GFP-ALFY$_{2981–3526}$. As can be seen in Fig 3G, the interaction with GABARAP was drastically reduced, whereas no increased affinity towards LC3B was detected, indicating that these ALFY residues provide selective binding to GABARAP, rather than block the interaction with LC3B. Taken together, we conclude that while the core LIR residues of ALFY are essential for its interaction with GABARAP, additional residues outside the core LIR motif confer specificity to the interaction of ALFY with GABARAP.

GABARAP is required for recruitment of LC3B to ALFY-positive structures and for the clearance of ALFY-p62-positive bodies

We have previously found that ALFY is recruited to cytoplasmic Ub- and p62-positive bodies upon stress such as amino acid starvation, proteasomal inhibition and puromycin treatment [4,12]. We here show that endogenous LC3B (Supplementary Fig S3), as well as stably expressed GFP-GABARAP (Fig 4A), colocalized with endogenous ALFY in stress-induced cytoplasmic structures. Interestingly, full-length wild-type GFP-ALFY, but not the LIR mutant, was recruited to GABARAP and LC3B-positive structures when expressed in ALFY-deficient MEFs (Fig 4B and Supplementary Fig S4). As ALFY does not interact with LC3B, and has very low affinity for LC3C, which is not present in mice and expressed at very low levels in HeLa and Hek293 cells (Unpublished data and Supplementary Fig S5A), we conclude that interaction of ALFY with GABARAP is required for its colocalization with LC3B. In line with this, while overexpressed ALFY$_{2285–3526}$ did not colocalize with wild-type GFP-LC3B, colocalization was observed upon the induction of excess GABARAP (Supplementary Fig S5B) or expression of the GFP-LC3B (Q26K/H27Y/H57D) mutant (Supplementary Fig S5B), indicating that the structural determinants identified as being important for GABARAP-ALFY binding specificity also determine colocalization between these proteins. GFP-GABARAP, -LC3B and -LC3B (Q26K/H27Y/H57D) stably expressed in these cell lines were considered functional as they retained the ability to become lipidated (Supplementary Fig S6A).

Further supporting a role of GABARAP in recruiting LC3B-positive membranes to ALFY-positive structures, we found an accumulation of ALFY-p62-positive structures that were negative for LC3B in GABARAP-depleted cells, whereas ALFY-p62-LC3B-positive structures were seen in control cells (Fig 4C). Interestingly, p62- and LC3B-positive puncta lacking ALFY could be detected in siGABARAP cells (Fig. 4C). Thus, our data indicate that a subset of p62-positive structures localizes with LC3B in the absence of GABARAP, but that recruitment of LC3B to ALFY-p62 positive bodies, or *vice versa*, requires GABARAP. We have previously found that ALFY is required for packing of p62 oligomers into larger p62 bodies, as well as for their clearance by autophagy [4]. Consistent with this, the accumulation of Triton X-100-insoluble p62 seen in cells where autophagic flux was inhibited by bafilomycin A1 was prevented both in ALFY-depleted HeLa cells (Fig 4D) and in ALFY KO MEFs (Fig 4E). Taken together, our results argue that the ALFY-GABARAP interaction is important for targeting of certain p62 structures for clearance by autophagy (Fig 4F). In line with our previous data [5], depletion of ALFY did neither affect the total level, the lipidation nor the turnover of Atg8 proteins (LC3B, GABARAP and GABARAPL1) in response to starvation (Supplementary Fig S6B).

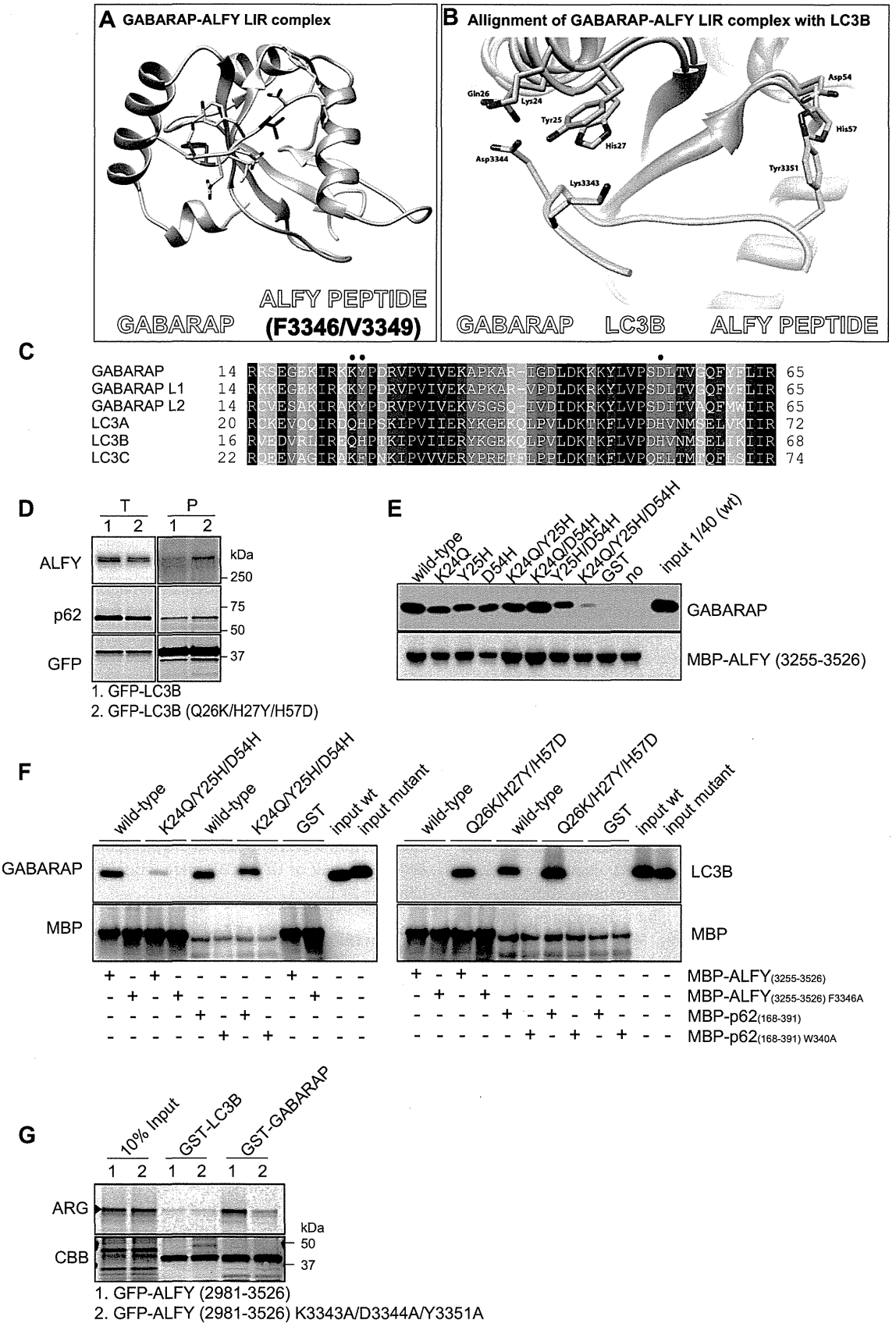

Figure 3. Structural analysis of GABARAP-ALFY peptide complex.

A Overall structure of the complex formed by GABARAP in brown and the ALFY-LIR peptide in yellow with the core LC3-interacting region (LIR) motif highlighted in dark blue.

B Alignment of the GABARAP-ALFY-LIR peptide complex structure with the published structure of LC3B (1UGM), using UCSF Chimera. See Supplementary Fig S2C and D for calculation of the distances between the residues highlighted as sticks in the ALFY-LIR peptide and the corresponding annotated residues in GABARAP or LC3B.

C Sequence alignment of human Atg8 protein homologs. The alignment was obtained by Clustal W. Black and grey backgrounds represent degree of similarity. Closed circles indicate specific residues of GABARAP involved in the ALFY-LIR peptide interaction.

D GFP-LC3B and GFP-LC3B (Q26K/H27Y/H57D) were immunoprecipitated with GFP-TRAP® from total cell lysate of stably transfected HeLa FlpIn cells, followed by SDS–PAGE and immunoblotting with the indicated antibodies. Data are representative of three independent experiments.

E MBP-ALFY$_{3255–3526}$ conjugated to amylose resin was incubated with GST or the indicated GABARAP mutants. The pulled-down complexes were subjected to SDS–PAGE and visualized by immunoblotting with anti-MBP and anti-GABARAP antibodies. Data are representative of three independent experiments.

F MBP-tagged ALFY$_{3255–3526}$ and p62$_{168–391}$ or their corresponding LIR mutants (F3346A and W340A, respectively) were conjugated to amylose resin and incubated with purified GST, GABARAP, GABARAP mutant (K24Q/Y25H/D54H), LC3B or LC3B mutant (Q26K/H27Y/H57D). The bound proteins were visualized by immunoblotting with anti-GABARAP, anti-LC3 and anti-MBP antibodies. Data are representative of three independent experiments.

G ^{35}S-labelled *in vitro*-translated GFP-ALFY (aa 2981–3526) wild-type and K3343A/D3344A/Y3351A mutant were incubated with GST-LC3B and GABARAP and binding evaluated by ARG. 10% of the *in vitro*-translated proteins used was loaded. CBB staining shows equal amounts of GST proteins used. Data are representative of three independent experiments.

Source data are available online for this figure.

Although the precise function of the different Atg8 homologs largely remains to be characterized, they have all been implicated in autophagy, either by recruiting cargo through their interaction with autophagy receptor proteins or by facilitating different steps of autophagosome biogenesis [2]. However, many open questions remain to be addressed, as whether LC3/GABARAP proteins act by recruiting different types of cargo or cooperate in cargo recruitment by binding different cargo-bound autophagy receptors, or whether they function sequentially in the pathway or in response to various types of stimuli.

In contrast, an extensive effort over the past few years has led to the identification of several LC3/GABARAP-interacting proteins, determination of LIR/CLIR motifs and functional characterization of many such proteins. It seems clear that while cargo-recruiting autophagy receptors (e.g. p62, NBR1 and optineurin) are specifically recruited to the inner surface of the phagophore and themselves become degraded by autophagy [13–15], other proteins (e.g. Rab effectors) associate in a LIR-dependent manner to the outer surface of the autophagosomes to facilitate their transport [16–18]. A third group of Atg8-interacting proteins (e.g. ULK1 complex proteins) [19] seems to be involved in scaffolding of protein complexes to allow their interaction with the phagophore membrane, without being themselves degraded by autophagy. We speculate that ALFY belongs to the latter group, as it is required for the recruitment of core Atg proteins to p62-positive protein aggregates, without becoming degraded by autophagy itself (Fig 4F) [4,5]. Interestingly, similar to ALFY, ULK1 complex proteins were found to interact preferentially with GABARAPs through FxxV/I LIR motifs, and their LIR-dependent interactions with GABARAP seem to facilitate their recruitment to LC3B-positive structures [19]. How and when these Atg8-interacting proteins are eventually released from the forming autophagosome is not known, but a regulation of their interaction with GABARAP is likely involved.

Materials and Methods

The experimental procedures, as well as plasmids used (Supplementary Table S2), are described in detail in the supplementary information online.

Cell culture

HeLa, U2OS and MEFs were used for transfection of constructs or siRNA. FlpIn T-Rex™ HeLa cells with stable inducible expression of GFP-GABARAP or GFP-LC3B were induced with 500 ng/ml tetracycline for 24 h.

Immunofluorescence microscopy

Confocal images were acquired on an Olympus FluoView 1000 confocal laser-scanning microscope. Image processing and analysis

Figure 4. Physiological role of the interaction between ALFY and GABARAP.

A HeLa FlpIn GFP-GABARAP cells were treated with proteasomal inhibitor (MG132, 2 h) or subjected to amino acid starvation (EBSS, 2 h), before staining with anti-ALFY antibodies. Scale bar, 10 μm.

B GFP-tagged full-length ALFY wild-type or LC3-interacting region (LIR)-mutant was expressed into *Alfy*-deficient MEFs using an adenovirus system. At 48 h after infection, the MEFs were cultured in normal media or EBSS for 1.5 h before staining with anti-LC3B or anti-GABARAP antibodies. Scale bars 10 μm.

C HeLa cells were treated with control or siRNA targeting GABARAP, GABARAPL1 and GABARAPL2. 72 h after transfection cells were immunostained with anti-LC3B, anti-ALFY and anti-p62 antibodies. Scale bars, 10 μm.

D HeLa cells were treated with control or siRNA targeting ALFY. 72 h after transfection, cells were treated with puromycin with or without bafilomycin A1 for 2 h and total cell lysates were fractionated into TX-100-soluble and insoluble fractions. The TX-100-soluble/insoluble fractions were then immunoblotted with the indicated antibodies. Data are representative of three independent experiments.

E ALFY WT and KO MEFs were treated with puromycin or EBSS with or without bafilomycin A1 for 2 h and the total cell lysates were then fractionated into Triton X-100 (TX-100)-soluble and insoluble fractions. The TX-100-soluble/insoluble fractions were then immunoblotted with the indicated antibodies. Data are representative of three independent experiments.

F Schematic model of ALFY-mediated selective autophagy.

Source data are available online for this figure.

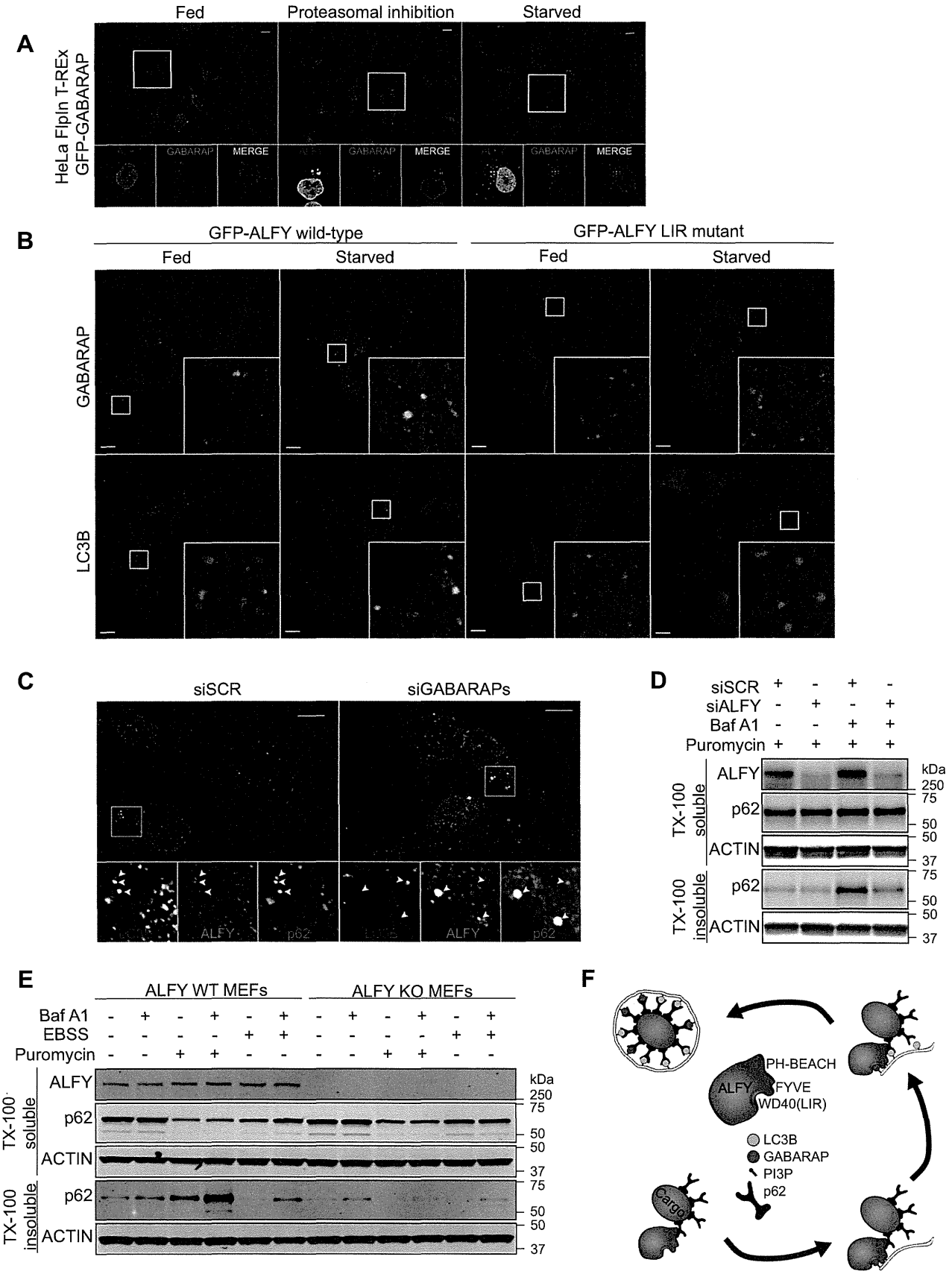

were done with OLYMPUS FLUOVIEW Viewer software and Adobe Photoshop CS4 (Adobe Systems).

In vitro pull-down assays

GFP- and STREP-FLAG-tagged proteins were pulled down using GFP-TRAP, μMACS (Miltenyi Biotec) or Strep-Tactin Sepharose (IBA). ^{35}S-methionine-labelled *in vitro*-translated GFP-tagged proteins were mixed with GST-tagged Atg8 proteins bound to glutathione Sepharose (GE Healthcare Bio-Sciences). For direct binding assays, MBP-tagged proteins were pulled down with GST-tagged proteins. Alternatively, precision protease was used to cleave off the GST tag before their incubation with recombinant MBP proteins and precipitation with amylose resin (New England Biolabs).

Crystal structure

The crystal structure of the GABARAP-ALFY peptide complex (PDB ID code 3WIM) was solved by molecular replacement using the structure of wild-type GABARAP (PDB ID code 1GNU) as the search model.

Supplementary information for this article is available online: http://embor.embopress.org

Acknowledgements
We thank T. Mita (Tokyo Metropolitan Institute of Medical Science) for his help with cell biological and biochemical studies, A. Kunida (University of Tokyo) for digital PCR analysis and all members of beamline BL44XU for help in data collection at SPring-8. This work was supported by grants from the Research Council of Norway and the Norwegian Cancer Society (to AS) and from a Grant-in-Aid for Scientific Research on Innovative Areas (to MK).

Author contributions
AHL, SP, MK and AS designed the experiments; AHL, YI, YY, SK and SP carried out the biochemical and cell biological experiments; KT, TM and AS completed the structural analysis; YK, MS and IS made the adenovirus vectors; AHL, SP and AS analysed the data; AHL, TM, MK and AS wrote the manuscript. All authors discussed the results and commented on the manuscript.

Conflict of interest
The authors declare that they have no conflict of interest.

References

1. Johansen T, Lamark T (2011) Selective autophagy mediated by autophagic adapter proteins. *Autophagy* 7: 279–296
2. Shpilka T, Weidberg H, Pietrokovski S, Elazar Z (2011) Atg8: an autophagy-related ubiquitin-like protein family. *Genome Biol* 12: 226
3. von Muhlinen N, Akutsu M, Ravenhill BJ, Foeglein A, Bloor S, Rutherford TJ, Freund SM, Komander D, Randow F (2012) LC3C, bound selectively by a noncanonical LIR motif in NDP52, is required for antibacterial autophagy. *Mol Cell* 48: 329–342
4. Clausen TH, Lamark T, Isakson P, Finley K, Larsen KB, Brech A, Overvatn A, Stenmark H, Bjorkoy G, Simonsen A et al (2010) p62/SQSTM1 and ALFY interact to facilitate the formation of p62 bodies/ALIS and their degradation by autophagy. *Autophagy* 6: 330–344
5. Filimonenko M, Isakson P, Finley KD, Anderson M, Jeong H, Melia TJ, Bartlett BJ, Myers KM, Birkeland HC, Lamark T et al (2010) The selective macroautophagic degradation of aggregated proteins requires the PI3P-binding protein Alfy. *Mol Cell* 38: 265–279
6. Finley KD, Edeen PT, Cumming RC, Mardahl-Dumesnil MD, Taylor BJ, Rodriguez MH, Hwang CE, Benedetti M, McKeown M (2003) blue cheese mutations define a novel, conserved gene involved in progressive neural degeneration. *J Neurosci* 23: 1254–1264
7. Knight D, Harris R, McAlister MS, Phelan JP, Geddes S, Moss SJ, Driscoll PC, Keep NH (2002) The X-ray crystal structure and putative ligand-derived peptide binding properties of gamma-aminobutyric acid receptor type A receptor-associated protein. *J Biol Chem* 277: 5556–5561
8. Stangler T, Mayr LM, Willbold D (2002) Solution structure of human GABA(A) receptor-associated protein GABARAP: implications for biological function and its regulation. *J Biol Chem* 277: 13363–13366
9. Ichimura Y, Kumanomidou T, Sou YS, Mizushima T, Ezaki J, Ueno T, Kominami E, Yamane T, Tanaka K, Komatsu M (2008) Structural basis for sorting mechanism of p62 in selective autophagy. *J Biol Chem* 283: 22847–22857
10. Satoo K, Noda NN, Kumeta H, Fujioka Y, Mizushima N, Ohsumi Y, Inagaki F (2009) The structure of Atg4B-LC3 complex reveals the mechanism of LC3 processing and delipidation during autophagy. *EMBO J* 28: 1341–1350
11. Rogov VV, Suzuki H, Fiskin E, Wild P, Kniss A, Rozenknop A, Kato R, Kawasaki M, McEwan DG, Lohr F et al (2013) Structural basis for phosphorylation-triggered autophagic clearance of Salmonella. *Biochem J* 454: 459–466.
12. Simonsen A, Birkeland HC, Gillooly DJ, Mizushima N, Kuma A, Yoshimori T, Slagsvold T, Brech A, Stenmark H (2004) Alfy, a novel FYVE-domain-containing protein associated with protein granules and autophagic membranes. *J Cell Sci* 117: 4239–4251
13. Pankiv S, Clausen TH, Lamark T, Brech A, Bruun JA, Outzen H, Overvatn A, Bjorkoy G, Johansen T (2007) p62/SQSTM1 Binds Directly to Atg8/LC3 to facilitate degradation of ubiquitinated protein aggregates by autophagy. *J Biol Chem* 282: 24131–24145
14. Kirkin V, Lamark T, Sou YS, Bjorkoy G, Nunn JL, Bruun JA, Shvets E, McEwan DG, Clausen TH, Wild P et al (2009) A role for NBR1 in autophagosomal degradation of ubiquitinated substrates. *Mol Cell* 33: 505–516
15. Wild P, Farhan H, McEwan DG, Wagner S, Rogov VV, Brady NR, Richter B, Korac J, Waidmann O, Choudhary C et al (2011) Phosphorylation of the autophagy receptor optineurin restricts Salmonella growth. *Science* 333: 228–233
16. Pankiv S, Alemu EA, Brech A, Bruun JA, Lamark T, Overvatn A, Bjorkoy G, Johansen T (2010) FYCO1 is a Rab7 effector that binds to LC3 and PI3P to mediate microtubule plus end-directed vesicle transport. *J Cell Biol* 188: 253–269
17. Itoh T, Kanno E, Uemura T, Waguri S, Fukuda M (2011) OATL1, a novel autophagosome-resident Rab33B-GAP, regulates autophagosomal maturation. *J Cell Biol* 192: 839–853
18. Popovic D, Akutsu M, Novak I, Harper JW, Behrends C, Dikic I (2012) Rab GTPase-activating proteins in autophagy: regulation of endocytic and autophagy pathways by direct binding to human ATG8 modifiers. *Mol Cell Biol* 32: 1733–1744
19. Alemu EA, Lamark T, Torgersen KM, Birgisdottir AB, Larsen KB, Jain A, Olsvik H, Overvatn A, Kirkin V, Johansen T (2012) ATG8 family proteins act as scaffolds for assembly of the ULK complex: sequence requirements for LC3-interacting region (LIR) motifs. *J Biol Chem* 287: 39275–39290